5-14-2021

Spectrum Modeling of RF Amplifiers Based on Intercept Points with Measurement Improvements

Siyuan Yan
Portland State University

Spectrum Modeling of RF Amplifiers Based on Intercept Points with Measurement Improvements

by

Siyuan Yan

A dissertation submitted in partial fulfillment of the
requirements for the degree of

Doctor of Philosophy
in
Electrical and Computer Engineering

Dissertation Committee:
Fu Li, Chair
Xiaoyu Song
Donald Duncan
Dacian Daescu

Portland State University
2021

Abstract

Orthogonal frequency-division multiplexing has been developed into a popular modulation scheme for wireless communication systems, used in applications such as LTE and 5G. In wireless communication system, spectrum regrowth caused by RF amplifiers will generate distortions to both passband in use and adjacent channels such that the transmission quality will be degraded. The study of this dissertation aims to predict the spectrum regrowth for OFDM based signals at the output of a RF amplifier due to the nonlinearity. Based on Taylor polynomial coefficients, a power spectrum expression for amplified OFDM signals in terms of intercept points up to n^{th}-order is derived. This model is useful to RF engineers in choosing the testing RF amplifiers with appropriate specifications, such as intercept points and gain, to meet the requirements of wireless standards. The proposed model is confirmed by the measurement results.

For predicting spectrum regrowth accurately with the proposed method, the key parameter, intercept points, need to be correctly determined. IP_3 is an important figure of merit for describing the nonlinearity of RF amplifiers. It is available from the datasheet and calculated from the interception between the line of the output power at fundamental frequencies versus the input power and the line of the power of the 3^{rd}-order intermodulation product conventionally measured from a two-tone test. However, the measured output power at fundamental frequency is not only from the fundamental tones, but also affected by 3^{rd}-order intermodulation products. As the input power further increases, the higher-order intermodulation becomes visible, which might affect the measurements at the frequencies of fundamental tones and of lower-order

intermodulation products. Thus, a similar issue arises for the intercept point measurements beyond 3rd-order. In this dissertation, starting with a two-tone test, the impacts from 3rd-order IM products to fundamental tones are analyzed. The measured IP_3 is thus corrected by removing the 3rd-order IM impacts at fundamental frequencies. The measurement improvements on intercept points of different orders using higher-order IM measurements are then derived. As higher-order IM products are usually far less than 3rd-order IM products, higher-order intercept points are of less importance. Thus, in the experimental measurements, the IP_3 comparison between the result of the conventional method and that of the corrected method correction is explained and analyzed, which verifies the method is necessary. By using the improved IP_3 from measurements, the corresponding adjacent channel power ratio can be calculated accurately, which is useful to RF amplifier design and testing in compliance with 5G standards.

Acknowledgements

It would have been impossible to complete this dissertation without the help and support of the kind and bright people around me. I have been very fortunate to meet and work with them.

First of all, I would like to express my sincere gratitude and deepest appreciation to my advisor and dissertation committee chair, Professor Fu Li, for his dedicated support, encouragement, guidance, and trust throughout my entire Ph.D. study. He has taught me not only the method to conduct research but also the wisdom of living, which has established the basis that could lead me to future success. He has always been available to provide me timely and invaluable advice. I couldn't have asked for more from my advisor.

Next, I would like to express my deepest appreciation to Professors Xiaoyu Song, Donald Duncan, and Dacian Daescu for serving on the dissertation committee and their insightful comments on my dissertation. My appreciation is also extended to Professor Donald Duncan for his guidance on my graduate teaching assistantship for four years.

Furthermore, I owe special thanks to Xianzhen Yang, my peer and fellow Ph.D. student in our VIP (video and information processing) lab, for his cooperation in our theme research for the past several years. I am also grateful to Dr. Xiao Li for his help on experimental set-up and research, and his mentoring during my internships at Tektronix. And thanks to Dr. Qiang Wu, Dr. Heng Xiao, and Professor Bruno Jedynak for their insightful comments and suggestions on my research. I would like to recognize the assistance that I received from Linnea Spitzer and the PSU writing center for

improving the manuscripts' writing.

My special thanks to my fellow students at Portland State University: Zhe Lu, Lai Xu, Yiwei Li, Ding Luo, Peng Chen, Katlin Dahn, and Jann Messer. Their friendships give me the courage to overcome the loneliness during my study.

Finally, from the bottom of my heart, I would like to thank my wife and parents for their love and support.

Table of Contents

List of Tables

List of Figures

Abbreviation List

3GPP	The third-generation partnership
4G	Fourth Generation Mobile Communication
5G	Fifth Generation Mobile Communication
ACPR	Adjacent channel power ratio
AM-AM	Amplitude modulation to amplitude modulation
AM-PM	Amplitude modulation to phase modulation
DSL	Digital subcarrier line
eMBB	Enhanced mobile broadband
FBMC	Filter bank multi-carrier
F-OFDM	Filtered orthogonal frequency-division multiplexing
HD	Harmonic distortion
IEEE	Institute of Electrical and Electronics Engineers
IM	Intermodulation
IMD	Intermodulation distortion
IP_3	3^{rd}-order intercept point
LNA	Low noise amplifier
LTE	Long-term evolution
mMTC	Massive machine type communications
OFDM	Orthogonal frequency-division multiplexing
OOB	Out-of-band
PA	Power amplifier

PSD	Power spectrum density
SEM	Spectrum emission mask
THD	Total harmonic distortion
URLLC	Ultrareliable low latency communications

Chapter 1 Introduction

1.1 Research Background and Motivation

Orthogonal frequency-division multiplexing (OFDM) is the most popular multi-carrier scheme which is curretly been deployed in board class of digital subcarrier line (DSL) standards [1] [2], as well as in majority of wireless standards [3], such as variations of IEEE 802.11 and IEEE 802.16, the third-generation partnership long-term evolution (3GPP-LTE), 4G LTE-advanced, and 5G, due to its immunity to selective fading, high spectrum efficiency, simpler channel equalization, and low complexity of implementation [4]. OFDM is also considered as one of the significant candidates for future communication systems [5] [6]. However, the emerging and future communication systems will be sensitive to nonlinear distortions caused by RF amplifiers in RF wireless communication systems.

In 5G wireless communication systems, the demands of millimeter-wave beamforming front-end intergrated circuits are increasing [7]-[10]. RF amplifiers including RF amplifiers including RF power amplifier (PA) and low noise amplifier (LNA) are critical and costly components in the front-end systems because their specifications strongly impact the system-level performance of the complete transceivers [11]. One of the concerns of RF amplifiers is the nonlinear distortions which manifest both channels in use and adjacent. These distortions will degrade the transmission quality, increase bit error rate, interference to adjacent channels, and violate the emission requirements. Therefore, it is important to quantify the nonlinearity prior to the compensation such that analytical expressions are necessary for power

spectra.

Due to the nonlinearity, extra frequemcy components, known as intermodulation (IM) products, are often degrade the performance of the communication transmission. IM has always been present in RF amplifiers. Traditionally, third-order intercept point (IP_3) is the parameter which gauges the nonlinearity for RF amplifiers. In many cases, IP_3 is sufficient to describe the nonlinearity of RF amplifiers [12]. In [13], an analytical expression of the amplified output spectrum using IP_3 and gain of RF amplifiers is developed. When the input power is high, 5^{th}-order or even higher-order IM products might be visible such that IP_5 or even higher-order intercept points might be needed to describe high nonlinearity. [14] expressed the output spectrum regrowth in terms of the IP_3, IP_5, and gain. Further increasing the power of input signal, higher- (beyond fifth-) order distortions may be worthy exploring because they now might be above the noise floor [15]. In the latter case, IP_n ($n > 5$) might be considered to estimate higher-order distrotions. In this situation, [16] proposed a general amplified spectrum model based on n^{th}-order IM products. However, the Taylor coefficients used in the final spectrum expression need to solved in a set of equations which includes n^{th}-order IM products measurement, which is complicated to use. In addition, the approach in [16] for obtaining the output complex envelope of n^{th}-order IM products includes extra terms of Taylor series coefficients, which causes the result of power spectra inaccurate.

Therefore, a simpler and more accurate output spectrum model is needed.

1.2 Contributions

In this dissertation, an explicit expression by relating an estimation of output spectrum of an RF amplifier to its parameters IP_n was developed. The spectrum model provides the insights into explaining how nonlinearity affects adjacent channel power ratio (ACPR) and spectrum emission mask (SEM).

Since the parameters IP_n will be used in this spectrum model, obataining accurate IP_n will help RF designers to predict the output spectrum of RF amplifiers more accurately. Conventionally, IP_3 is calculated via a two-tone test measurement [17]. However, the measured output power at fundamental frequencies is not only attributed to the linear amplification, but also attributed to the third-order IM products. As the input signal further increases, the higher-order IM might become visible, which will have an impact directly to the measurements at fundamental frequencies and to the lower IM products. Therefore, the similar issue arises for the intercept points measurement beyond third-order.

Therefore, this research has been further conducted for correcting IP_n measurements. The impacts from higher-order IM products to the lower-order IM products and fundamental two tones by two-tone test measurements are analyzed. And corrections for the conventional method of measuring intercept points by removing corresponding impacts from the higher-order IM products are suggested. With improving the measurments of IP_3, the corresponding ACPR can be claculated [18] more accurately, which is useful to RF amplifier design and testing in compliance with 5G standards.

1.3 Dissertation Organization

This dissertation is organized as follows:

Chapter 2: A comprehensive review of the nonlinearity of RF amplifiers. The classes of RF amplifier operation and the tradeoff between the efficiency and linearity of RF amplifiers are discussed. Harmonic distortions and intermodulation distortions are explained. Nonlinear parameters, such as intercept points and 1dB compression point, are presented with one-tone tests and two-tone tests, respectively.

Chapter 3: A detailed derivation of n^{th}-order spectrum model. Several prior models of power spectrum are reviewed and evaluated. A spectrum model which is related to n^{th}-order intercept point of RF amplifiers is proposed. Measurements are carried out to validate the results of the proposed model.

Chapter 4: Improving the measurements of intercept point. The impacts from 3^{rd}-order IM products to fundamental tones are analyzed. The conventionally measured IP_3 is corrected by removing corresponding 3^{rd}-order IM products. Descriptions on improving intercept points of different orders using higher-order IM measurements are derived. Experiments are carried out to verify the correction methods.

Chapter 5: A summary of all the results included in this dissertation. Further research works and approaches are proposed.

Chapter 2 Nonlinearity of RF Amplifiers

In wireless communication systems, two components, the low-noise amplifier and power amplifier, are the critical interfaces between the antennas and the electronic circuits which are shown in Figure 2.1 [19]. LNAs and PAs will be at opposite ends of an RF link. At the front end of the receiver channel [20], LNAs will capture and amplify low power signal of interest with associated random noise via antennas. In contrary, PAs will take relatively a strong signal from the circuits with a high SNR and boost the input power. In a duplex system, the LNA and PA usually connect to a duplexer instead of the antenna directly. The duplexer is a device that allows bi-directional communication over a single channel, which will be used to isolate the receiver from the transmitter while permitting them to share a common antenna in wireless communication systems.

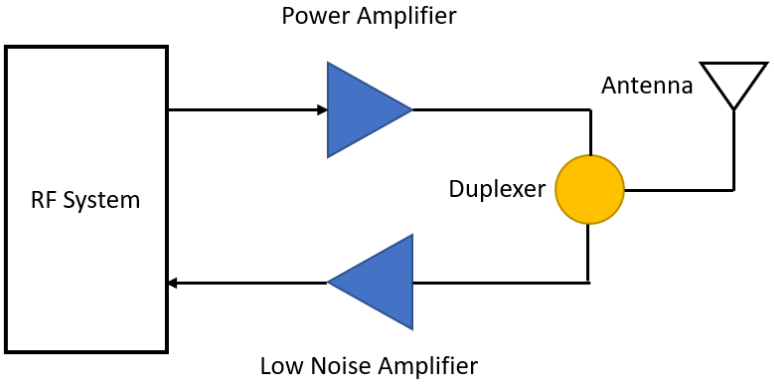

Figure 2.1. The LNA of the receiver channel and the PA of the transmitter channel connect to the antenna via a duplexer.

2.1 Classes of RF Amplifier Operation

Generally, a practical RF amplifier is a linear device only in its linear region (low-level region). The efficiency and linearity of RF amplifiers are both the key specifications. The efficiency of RF amplifiers is the ratio of RF output power to DC input power, which can be described as [21] [22]

$$\eta = \frac{P_{\text{out}}}{P_{\text{DC}}} = \frac{P_{\text{out}}}{V_{\text{DC}} \times I_{\text{DC}}} \tag{2.1}$$

where P_{out} is the RF output power delivered to the load, P_{DC} is the DC power from supply, V_{DC} is the power across the power supply, and I_{DC} is the current out from the power supply. The linearity refers to the essential job of an RF amplifier, which is to increase the power level of an input signal without altering the content of the signal [23].

To save the expense costs of operations, RF amplifiers should ideally be as energy efficient as possible since electrical power usage is one of the highest operating costs for carriers. However, making an RF amplifier more efficient often means driving it to its saturation point. Usually, the modulated waveforms will be distorted at the saturation point. The trade-off between efficiency and linearity are common in RF amplifier design. Based on the application requirements for efficiency and nonlinearity, the RF amplifier class can be divided into two categories [24]-[27]: The first group contains high linear amplifiers which are usually used in communication application, such as class-A, class-AB, class-B, and class-C; the second group contains high efficient amplifiers, such as class-D, class-F and class-E. The second group of amplifiers is also known as switched mode amplifiers [28]. Since the first group is used in mobile and

microwave applications [24] more often, only the first group will be discussed in this section.

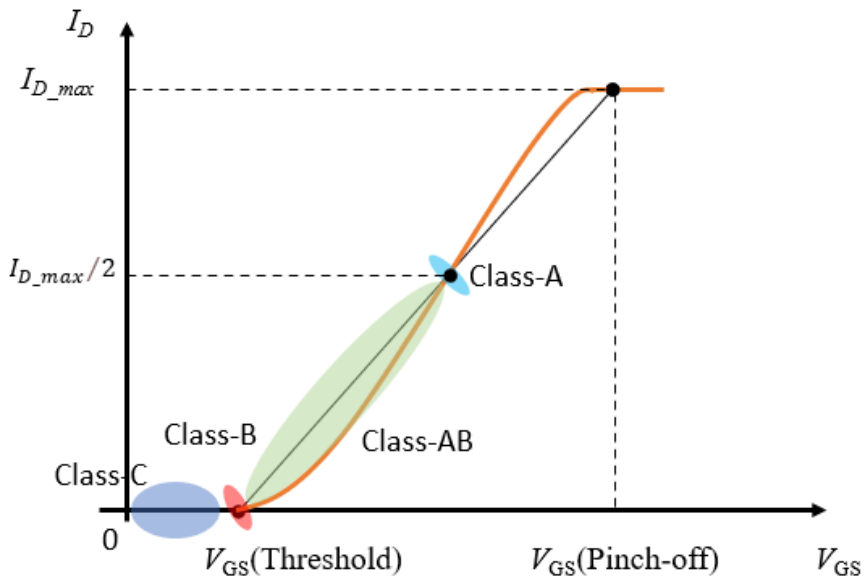

Figure 2.2. Operating point of amplifiers in first group.

In Figure 2.2, it is seen that the amplifier operation depends on the selection of transistor operating point which will affect the performance of RF amplifiers. I_D refers to the output current, V_{GS} (threshold) denotes the minimum gate to source voltage required to start conduction, and V_{GS} (pinch-off) denotes the gate to source voltage in which the drain current reaches maximum and becomes flat in the characteristic curve. It is seen that the transistor operation point of a class-A amplifier is chosen in the center of the linear region; the transistor operation point of a class-B amplifier is chosen close to the threshold voltage; the transistor operation point of a class-AB amplifier is chosen between class-A and class-B such that there is a flexible solution for a trade-off between linearity and efficiency; and the transistor operation point of a class-C amplifier is

chosen as the output current I_D is zero for more than one-half duration of the input signal cycle [29].

Class-A amplifiers have good linearity, and its theoretical maximum efficiency is 50%. Practically, the efficiency is typically around 30%. Class-B amplifier is less nonlinear as compared with class-A amplifier, but the theoretical maximum efficiency is 75%. Class-AB amplifier has better linearity than class-B amplifier and less linearity than class-A amplifier, and its theoretical maximum efficiency is around 60%. Last, class-C has the poorest linearity, and its theoretical maximum efficiency can catch up to 85% [30].

Since RF amplifiers have a major effect on the fidelity of wireless communications systems, large numbers of studies are undertaken to understand the limitations such that to optimize their performance. In general, the models of RF amplifiers can be divided into two major groups: physical models and behavioral (or empirical) models [31]. Physical models require knowledge of the electronic elements that constitute the RF amplifier, their relationships and the theoretical rules describing their interactions. However, when such an RF amplifier equivalent circuit is not available, or a complete system-level simulation is desired, the behavioral models are preferred [32] for analyzing the amplifiers.

Regardless of RF amplifiers' physical models, the task of RF amplifiers is to increase the power level of input signals at the given frequency. By the definitions in [17], small signal regime is defined as the linear region of RF amplifiers, and large signal regime is referred to as gain compression. To limit the power consumption, RF

amplifiers are typically operated under large signal regimes. Otherwise, a sufficiently large active device has to be adopted, resulting in an almost linear behavior, which will dissipate a large amount of DC power. Therefore, RF amplifier design is typically the result of a trade-off, trying to fulfil several conflicting requirements such as linearity versus efficiency, or high output power versus low distortion [17].

RF amplifier performs as a nonlinear system component, whose large-signal operating conditions often lead to detrimental effects on the output signal, resulting in a distorted replica of the input. The common nonlinear effects generated in RF amplifiers can be divided into memoryless nonlinear effects and memory nonlinear effects.

The emerging and future wireless communication systems will be sensitive to the distortions generated by the nonlinearity of RF amplifiers in the radio chain [33], which will impair channel efficiency and clarity of transmission. These distortions manifest both the channels in use and the adjacent channels. The following sections will discuss memoryless nonlinearity including harmonic distortion, AM-AM (amplitude modulation to amplitude modulation) and AM-PM (amplitude modulation to phase modulation) conversions, and intermodulation distortion, and memory nonlinearity.

2.2 Baseband and Bandpass Signal Definition

In communication system, the information source signal is usually a baseband signal. In order to transmit information from the source signal $m(t)$ to the desired destination, communication systems will be built by RF engineers. As shown in Figure

2.3 [34], $m(t)$ will be up converted to the bandpass signal $s(t)$ with carrier frequency f_c to propagate across the communication channel. The receiver then will receive $s(t)$ through annates and recover the information that was sent from the source.

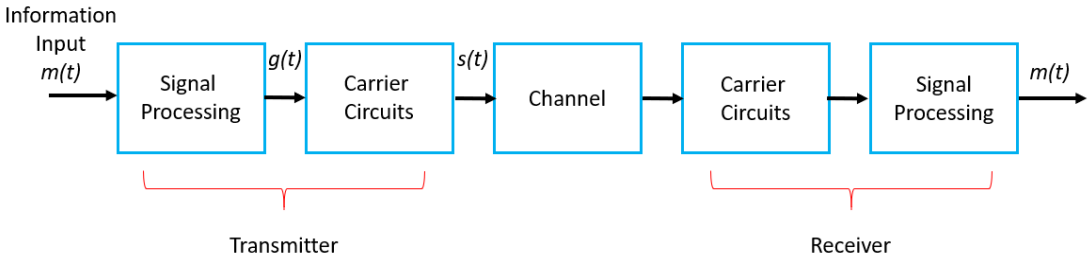

Figure 2.3. Communication system.

Any physical bandpass waveform can be represented by [34]

$$s(t) = \mathrm{Re}\left\{ g(t) e^{j\omega_c t} \right\} \tag{2.2}$$

where $\mathrm{Re}\{\cdot\}$ denotes the real part of $\{\cdot\}$, $g(t)$ is called the complex envelop of $s(t)$, ω_c is associated with the carrier frequency (in hertz), where $\omega_c = 2\pi f_c$. Furthermore, two other equivalent representations are

$$\begin{aligned} s(t) &= \tilde{s}(t)\cos[\omega_c t + \theta(t)] \\ &= I(t)\cos\omega_c t - Q(t)\sin\omega_c t \end{aligned} \tag{2.3}$$

where $\tilde{s}(t)$ denotes the amplitude, $\theta(t)$ denotes the phase, $I(t)$ denotes the in-phase component, and $Q(t)$ denotes the quadrature component.

RF amplifiers are devices which can increase the power of the transmitted signal. Ideally, RF amplifiers increase the power of the transmitted signal proportional to its gain following the form of [35] as

$$y(t) = G \cdot s(t) \tag{2.4}$$

where $s(t)$ is the input power, $y(t)$ is the output power with amplification, and G is the voltage gain of the RF amplifier. However, practical RF amplifiers will saturate beyond a certain value of input power due to their limited operation ranges such that the output of RF amplifier will not be exactly a scaled copy of the input signal when the amplifier works beyond the linear region due to nonlinearity. If a RF amplifier have poor linearity, it will generate harmonic and IM distortions at output.

A Taylor series model [36] has been widely adopted for describing the nonlinearities of RF amplifiers without memory effects, which can be described as

$$y(t) = \sum_{i=1}^{\infty} a_i s(t)^i = a_1 s(t) + a_2 s(t)^2 + a_3 s(t)^3 + \ldots \tag{2.5}$$

where a_i denotes the real value coefficients. For linear amplification, equation (2.5) could be reduced to $y(t) = a_1 s(t)$, which is the same as (2.4) ($a_1 = G$).

AM-AM characterization described the relation between the output amplitude of the fundamental frequency, with the input amplitude of a fixed input frequency. [37]. Thus, it characterizes gain compression or expansion of a nonlinear device versus input power level. AM-AM characterization enables the evaluation of an important figure merit named 1dB compression point, which will be discussed in the later section. AM-AM characterization is often expressed as a certain dB/dB deviation at a predetermined input power [38]

Another popular property of nonlinear systems is that vector addition of the output fundamental with distortion components also determines a phase variation of the

resultant output, as the input power level varies [39]. This is the AM-PM characteristics of nonlinear systems. AM-PM characterization consists of studying the variation of the output signal phase with input signal amplitude changes for a constant frequency, and may expressed as a certain phase deviation to $\theta(t)$ in (2.3), in degrees/dB, at a predetermined input power [38]. In this dissertation, only AM-AM characterization will be considered.

Since the analysis of multi-tone spectra can be very complicated, it is common to limit the analysis to a one-tone input signal or a two-tone input signal. Usually, the harmonic distortions can be measured by a single-tone test, and the IM distortions can be measured by a two-tone test.

2.3 One-tone test

Assuming the single-tone input signal is

$$s(t) = A \cdot \cos 2\pi f_c t \tag{2.6}$$

Substituting (2.6) into (2.5) yields to

$$y(t) = \sum_{i=1}^{\infty} a_i (A \cdot \cos 2\pi f_c t)^i \tag{2.7}$$

By simplifying (2.7) with trigonometric properties, the output signal will produce new frequency components which will locate at the harmonics (f_c, $2f_c$, $3f_c$, $4f_c$, …) as shown in Figure 2.4. P_t represents the power at the fundamental tone, P_n ($n \geq 2$) represents the power at the n^{th}-order harmonic frequency.

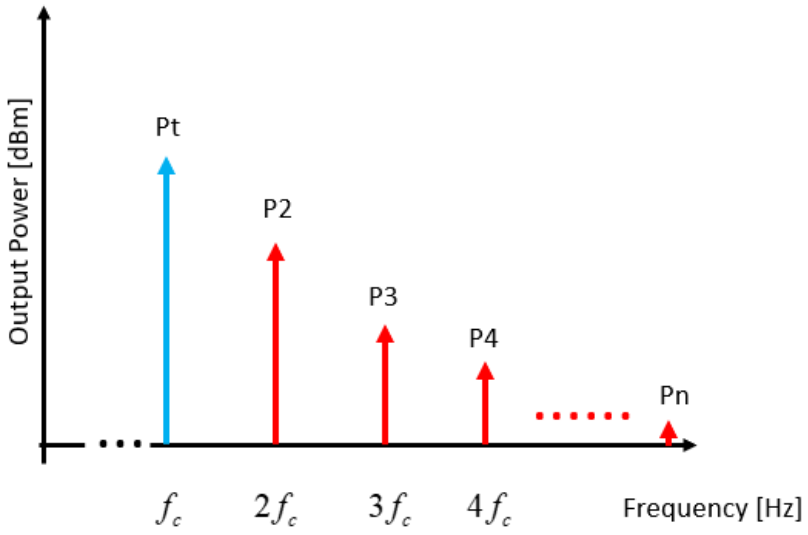

Figure 2.4. Harmonic distortion in a single-tone test.

With the single-tone test, we can measure the n^{th}-order harmonic distortion (HD_n) and calculate the total harmonic distortion (THD). This figure of merit is defined as the ratio between the square roots of total harmonic output power and output power at the fundamental signal as [40]

$$\text{THD} = \sqrt{\frac{P_2 + P_3 + \ldots + P_n + \ldots}{P_t}} \tag{2.8}$$

Combining (2.7) and (2.8), (2.9) can be rewritten as [39]

$$\begin{aligned} \text{THD} &= \sqrt{\frac{[\sum_{i=2}^{\infty} a_i (A \cdot \cos 2\pi f_c t)^i]^2}{[a_1 (A \cdot \cos 2\pi f_c t)]^2}} \\ &= \frac{1}{2}\frac{A}{a_1}\sqrt{a_2^2 + \frac{1}{4}a_3^2 A^2 + \ldots} \end{aligned} \tag{2.9}$$

Another type of nonlinear distortion, the intermodulation distortion, is usually measured by using a two-tone test, which will be discussed in the section 2.4.

2.4 Two-tone tests

As the nonlinearity within RF amplifiers generate other frequencies rather than harmonics, it is known as IM products. The nonlinearity of RF amplifiers will degrade the signal transmission quality and increase the interferences to the adjacent channels.

Assume the two-tone input signal as

$$s(t) = A_1 \cos 2\pi f_{c1} t + A_2 \cos 2\pi f_{c2} t \tag{2.10}$$

where A_1 and A_2 are the amplitudes of the two tones which centered at frequencies f_{c1} and f_{c2}, respectively. For simplifying the calculation, it is assumed that $A_1 = A_2 = A$. Substituting (2.10) into (2.5) with the assumption, the output signal can be expressed as

$$y(t) = \sum_{i=1}^{\infty} a_i (A \cdot \cos 2\pi f_{c1} t + A \cdot \cos 2\pi f_{c2} t)^i \tag{2.11}$$

Based on the conclusion derived from [24], the even-order terms are often far away from the center of the passband of interests such that they can be easily filtered. Therefore, the memoryless nonlinear model of RF amplifiers can be represented by odd-order Taylor series as

$$\begin{aligned} y(t) &= \sum_{n=1}^{\infty} a_{2n-1} (A \cdot \cos 2\pi f_{c1} t + A \cdot \cos 2\pi f_{c2} t)^{2n-1} \\ &= a_1 (A \cdot \cos 2\pi f_{c1} t + A \cdot \cos 2\pi f_{c2} t) \\ &\quad + a_3 (A \cdot \cos 2\pi f_{c1} t + A \cdot \cos 2\pi f_{c2} t)^3 + \ldots \\ &\quad + a_{2n-1} (A \cdot \cos 2\pi f_{c1} t + A \cdot \cos 2\pi f_{c2} t)^{2n-1} + \ldots \end{aligned} \tag{2.12}$$

where a_{2n-1} denotes the odd-order coefficients of Taylor series.

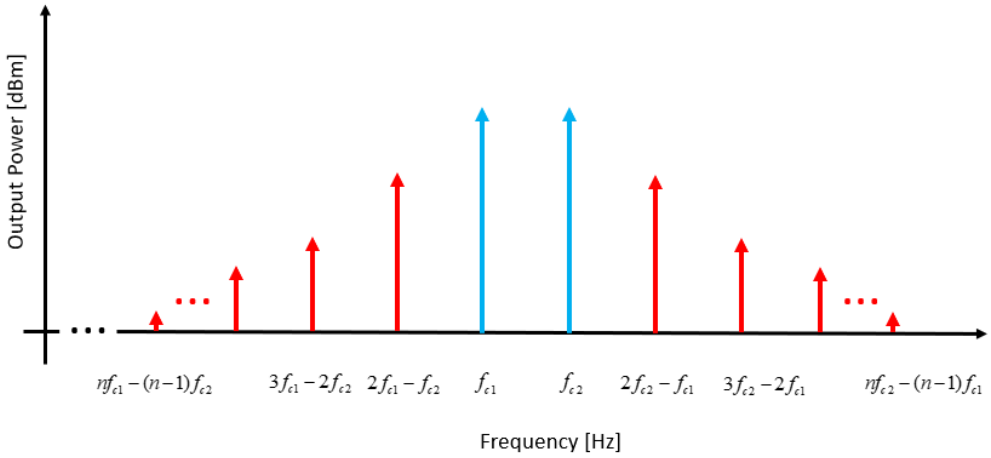

Figure 2.5. Intermodulation products in a two-tone test.

For the output bandpass signals, $a_1(A\cdot\cos 2\pi f_{c1}t + A\cdot\cos 2\pi f_{c2}t)$ is the term with linear amplification, and $a_{2n-1}(A\cdot\cos 2\pi f_{c1}t + A\cdot\cos 2\pi f_{c2}t)^{2n-1}$ ($n > 1$) is $(2n\text{-}1)^{\text{th}}$-order IM term. For a bandpass system, only the IM products locate at $[nf_{c1}-(n-1)f_{c2}]$ and $[nf_{c2}-(n-1)f_{c1}]$ fall within the passband and cannot be filtered out, which causes the IM distortion (IMD) as described in Figure 2.5. Intercept points are usually used to describe the IMD, the relation between the coefficients of Taylor series and intercept points is discussed in the section 2.5.2.

2.5 Specifications for Describing Nonlinearity

1dB compression point and 3rd-order intercept points (IP_3) are very important figures of merit which gauge nonlinearity of RF amplifiers, which is discussed below.

2.5.1 1dB Compression Point

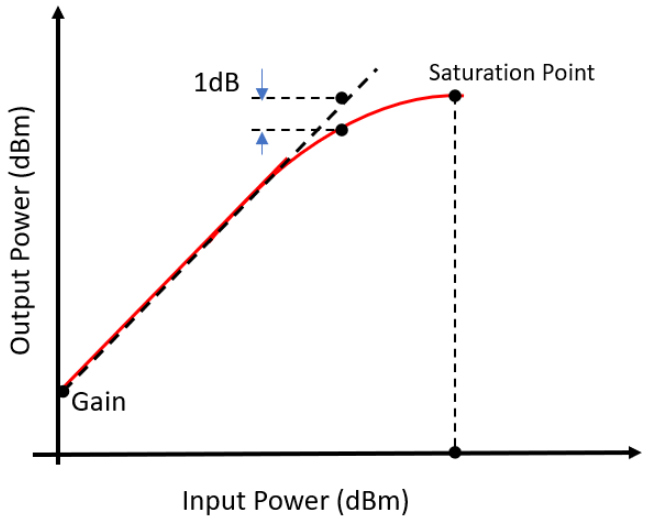

Figure 2.6. Definition of saturation point and 1dB compression point.

It is known that all RF amplifiers have maximum output power capacity, which is shown as saturated output power P_{sat} on actual nonlinear curve (the red solid curve) in Figure 2.6. The red solid curve describes the practical relation between P_{in} and P_{out}, and the black dash line describes the ideal linear relation between P_{in} and P_{out}. It is seen that the point where the difference between the black dash line and red solid curve equals to 1 dB is called 1 dB compression point $P_{1\text{dB}}$ [17].

In other word, the 1dB compression point is defined as the P_{out} at which the signal output is already compresses by 1dB, as compared to the output that would be obtained by simply extrapolating the linear system's small signal characteristic (linear region of red solid curve) as depicted in Figure 2.6. At this power level, the RF amplifiers have poor linearity, which will generate harmonics and IM products at output. Thus, amplifiers should be operated under this compression point. The corresponding

input power level of 1 dB compression point is used to mark the border between 'highly nonlinear' and 'almost linear' drive level regions [17].

When the distance between saturation point and 1 dB compression point reduces, the nonlinear region in Figure 2.6 will decrease resulting in the improvement of the linear properties of the amplifier.

2.5.2 Intercept Points

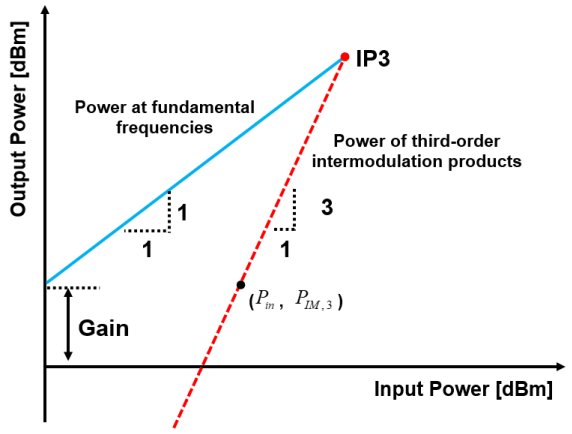

Figure 2.7. The point where the line of the power at fundamental frequency (slope 1) and that of the power of third-order intermodulation product (slope 3) meet is defined as third-order intercept point.

Third-order intercept points is a very important figure merit which gauges nonlinearity for RF amplifiers. It is defined as the intercept point between the line of the output power with linear amplification at fundamental frequencies versus input power, and that of power of 3rd-order IM products versus input power, as shown in Figure 2.7.

IP_3 is a fictitious point which is obtained when the extrapolated 1dB/dB slope line of the output fundamental power intersects the extrapolated 3-dB/dB slope line of the power of 3rd-order IM products [38].

In many cases, 3rd-order IM distortion is dominant and other higher-order IM distortions are neglectable, and IP_3 is sufficient to describe the nonlinearity of RF amplifiers. Considering 3rd-order nonlinear distortions only, equation (2.12) can be simplified as

$$\begin{aligned} y(t) &= a_1(A\cos 2\pi f_{c1}t + A\cos 2\pi f_{c2}t) + a_3(A\cos 2\pi f_{c1}t + A\cos 2\pi f_{c2}t)^3 \\ &= (a_1A + \frac{9}{4}a_3A^3)\cos 2\pi f_{c1}t + (a_1A + \frac{9}{4}a_3A^3)\cos 2\pi f_{c2}t \\ &+ \frac{3}{4}a_3A^3\cos(4\pi f_{c1} - 2\pi f_{c2})t + \frac{3}{4}a_3A^3\cos(4\pi f_{c2} - 2\pi f_{c1})t \\ &+ \frac{3}{4}a_3A^3\cos(4\pi f_{c1} + 2\pi f_{c2})t + \frac{3}{4}a_3A^3\cos(4\pi f_{c2} + 2\pi f_{c1})t \\ &+ \frac{1}{4}a_3A^3\cos 6\pi f_{c1}t + \frac{1}{4}a_3A^3\cos 6\pi f_{c2}t \end{aligned} \tag{2.13}$$

which consists of eight terms. The six terms in (2.13) which center at $2f_{c1} + f_{c2}$, $2f_{c2} + f_{c1}$, $3f_{c1}$, and $3f_{c2}$ fall outside the pass-band and can be filtered out by appropriate filters. Equation (2.13) can then be rewritten as

$$\begin{aligned} y(t) &= (a_1A + \frac{9}{4}a_3A^3)\cos 2\pi f_{c1}t + (a_1A + \frac{9}{4}a_3A^3)\cos 2\pi f_{c2}t \\ &+ \frac{3}{4}a_3A^3\cos(4\pi f_{c1} - 2\pi f_{c2})t + \frac{3}{4}a_3A^3\cos(4\pi f_{c2} - 2\pi f_{c1})t \end{aligned} \tag{2.14}$$

Note that the actual amplitude of the output signal at fundamental frequencies (f_{c1} or f_{c2}) is $a_1A + \frac{9}{4}a_3A^3$ where $a_3 < 0$ for gain compression. At low input power

levels (assuming $a_1 A \gg \frac{9}{4} a_3 A^3$), the output power $P_{f_{c1}}$ at f_{c1} or $P_{f_{c2}}$ at f_{c2} almost coincides with the response of the output power P_t at fundamental frequencies when the two-port is assumed to be linear. At higher power levels, the response of $P_{f_{c1}}$ will be compressed such that it will deviate from the blue solid line in Figure 2.7. With the linear amplification, the amplitude of either one of output fundamental tones is $a_1 A$. From [34] [39], the linear output power P_t can be expressed as

$$P_t = 10 \times \log[(\frac{a_1 A}{\sqrt{2}})^2 \frac{10^3}{R}] \quad \text{dBm} \tag{2.15}$$

where *R* is the input resistance. From (2.15), the power of 3rd-order IM products $P_{IM,3}$ can be derived as

$$P_{IM,3} = 10 \times \log[(\frac{\frac{3}{4} a_3 A^3}{\sqrt{2}})^2 \frac{10^3}{R}] \quad \text{dBm} \tag{2.16}$$

By the definition of IP_3, we know $P_t = P_{IM,3}$. Therefore, the theoretical amplitude at intersection in Figure 2.7 can be calculated by using (2.15) and (2.16) as

$$A^2 = \frac{4}{3} \times \frac{a_1}{|a_3|} \tag{2.17}$$

and therefore (assuming R=1)

$$\begin{aligned} IP_3 &= 10 \times \log[(\frac{a_1}{\sqrt{2}})^2 \cdot \frac{4}{3} \times \frac{a_1}{|a_3|} 10^3] \quad \text{dBm} \\ &= 10 \times \log(\frac{2}{3} \times \frac{a_1^3}{|a_3|} 10^3) \quad \text{dBm} \end{aligned} \tag{2.18}$$

In (2.19), coefficient a_1 is related to the gain *G* and linearity of the RF amplifier, which can be derived from the following equation [14]

$$a_1 = 10^{\frac{G}{20}} \tag{2.19}$$

After changing IP_3 scale from dBm to dB scale, with (2.18) and (2.19), we have

$$|a_3| = \frac{2}{3} 10^{(-\frac{IP_3}{10} + 3\frac{G}{20})} \tag{2.20}$$

In general, we choose $a_3 < 0$ for gain compression. In many cases, IP_3 is sufficient to describe the nonlinearity of RF amplifiers. When the input power is high, IP_5 or even higher-order intercept points might be needed. Traditionally, IP_3 will be given from the manufacturer's specifications. The higher-order intercept points are not generally provided, but they can easily be calculated from the power of IM products by using a two-tone test. In this dissertation, since the even-order IM distortions can be easily filtered such that the even-order intercept point will not be discussed.

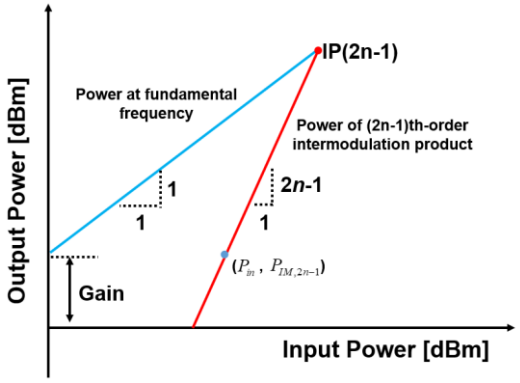

Figure 2.8. The point where the line of the power at fundamental frequency (slope 1) and that of the power of 3rd-order intermodulation product (slope (2*n*-1)) meet is defined as (2*n*-1)th-order intercept point.

Similar to the definition of IP_3, the $(2n\text{-}1)^{th}$-order intercept point (IP_{2n-1}) is defined as the output power level where the power of $(2n\text{-}1)^{th}$-order IM products (with slope $2n$-1) would intercept with the output power at fundamental frequencies as described in Figure 2.8. The two lines in this log-log scale plot will both be a straight line with a slope corresponding to the order of the output response [38].

As mentioned in section 2.2.3, only the odd-order IM products at $[nf_{c1}-(n-1)f_{c2}]$ and $[nf_{c2}-(n-1)f_{c1}]$ fall within the passband and cannot be filtered, which causes distortion. If the components out of the passband are filtered out, we can rewrite (2.12) as

$$\begin{aligned} y(t) &= b_1(\cos 2\pi f_{c1}t + \cos 2\pi f_{c2}t) \\ &+ b_3[\cos(4\pi f_{c1} - 2\pi f_{c2})t + A\cdot\cos(4\pi f_{c2} - 2\pi f_{c1})t] + \ldots \\ &+ b_{2n-1}\{\cos 2(n\pi f_{c1} - (n-1)\pi f_{c2}]t + \cos 2(n\pi f_{c2} - (n-1)\pi f_{c1}]t\} + \ldots \end{aligned} \tag{2.21}$$

By the definition of intercept points, the linear output power P_t can be expressed as (2.15), and the amplitude coefficient b_{2n-1} of the $(2n\text{-}1)^{th}$-order IM components is given by [17]

$$b_{2n-1} = \frac{1}{2^{2n-2}}\cdot\binom{2n-1}{n}\cdot a_{2n-1}\cdot A^{2n-1} \tag{2.22}$$

where $\binom{2n-1}{n}$ gives the number of different combinations of n elements that can be chosen from a $(2n$ -1)-element set. Based on (2.22) and the definition of intercept points, [41] proposed an expression that relates $(2n\text{-}1)^{th}$-order coefficient of Taylor series model in terms of the $(2n\text{-}1)^{th}$-order intercept point as

$$a_{2n-1} = -\frac{2^{n-1}}{\binom{2n-1}{n}} 10^{\left[\frac{-(2n-2)IP_{2n-1}+(2n-1)G}{20}\right]} \tag{2.23}$$

With (2.23), the spectrum analysis for multi-tone signals with arbitrary order now becomes possible, which will be introduced in Chapter 3.

2.6 Memory Effects

Memory nonlinear systems can be represented by nonlinear differential or memory polynomial equations such that the output signal will be a function of both the instantaneous and previous input signal. Memory effects can be categorized as electrical and thermal effects [29]. Figure 2.9 illustrates the main source of electrical memory and thermal memory in a power active device.

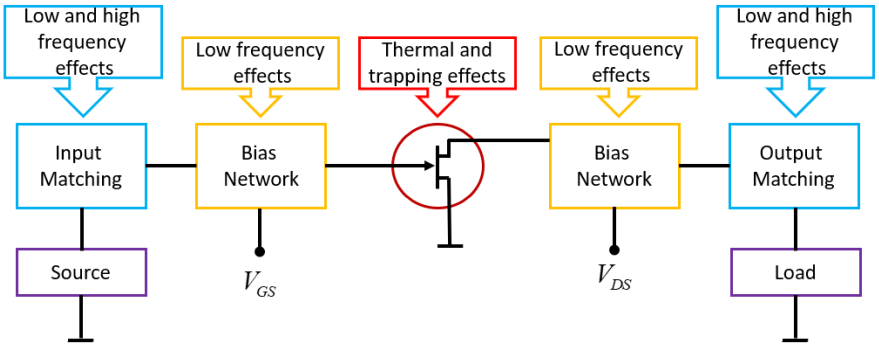

Figure 2.9. Typical sources of memory effects in RF amplifiers.

In a two-tone test, with memory effects, the output signal with amplification often shows a significant amount of asymmetry between the upper and lower IM products as shown Figure 2.10.

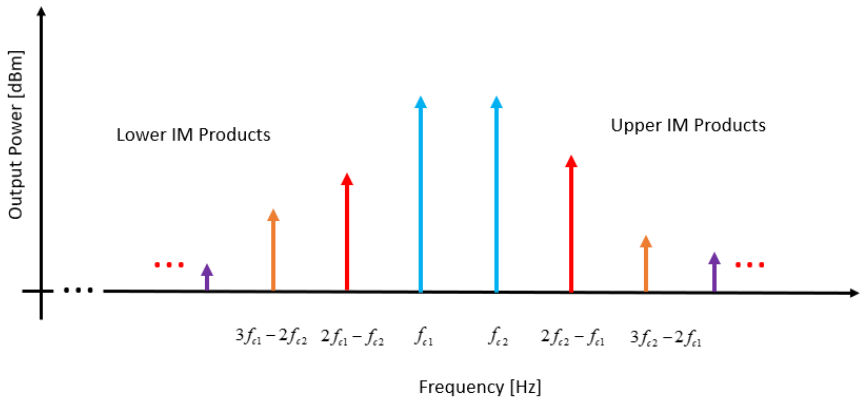

Figure 2.10. Two-tone test with memory effect.

Memory effects are often described by Volterra, Wiener, or Hammerstein model, and the coefficients of the non-constant distortion behavior have to be extracted from measurement. Therefore, it is difficulty in deriving explicit spectral model with memory effects. Therefore, in this dissertation, the impacts of memory nonlinearity on spectrum analysis will not be included.

Chapter 3 Spectrum Modeling in terms of Intercept points for RF amplifiers

Future wireless networks will be characterized by a large range of possible use cases, such as enhanced mobile broadband (eMBB), massive machine type communications (mMTC), and ultrareliable low latency communications (URLLC) [43] [39]. To efficiently support the diversity of use case, a flexible allocation of available time-frequency resources is needed [44].

OFDM is one of the most popular schemes for wideband digital communications. Due to the merits of the orthogonality, the closely spaced orthogonal subcarriers partition the available bandwidth into a collection of narrow subcarriers. Also, the adaptive modulation schemes can be applied to subcarrier bands to increase the overall bandwidth efficiency. OFDM provides high data rate transmission, robust multi-path fading and ease of implementation [4]. Thus, OFDM can be considered as one of the candidates. Although OFDM has been used in LTE-Advanced and 5G, it is still important to investigate the alternative filtered-based schemes which also meet the above requirements for future wireless systems, such as filter bank multi-carrier (FBMC), and filtered orthogonal frequency-division multiplexing (F-OFDM). In contrast to OFDM, F-OFDM applies a filtering functionality to each of the subbands which has more than one subcarrier. F-OFDM and FBMC both provide the lower out-of-band (OOB) emission and better time/frequency localization properties. These two schemes also gained lots of attention from the industry and academia.

As mentioned in chapter 2, single-tone tests and two-tone tests can be used to measure the harmonic distortions and IM distortions. However, those methods cannot

provide any insights into explaining how nonlinearities affect ACPR or SEM. In wireless communication systems, meeting spectral regulatory masks is mandatory [45] in compliance with 5G standards. Thus, the spectrum model is an important performance metric. In this chapter, we will first review several spectrum models. Then, a method for predicting the spectrum regrowth of amplified OFDM signals by using higher-order intercept points will be derived. At last, the presented analytical model is verified by experimental measurements.

3.1 Signal models and power spectrum

Based on [46] [47], the power spectrum density (PSD) of an OFDM or FBMC signal $s(t)$ can be expressed as

$$P_s(f) = \begin{cases} \frac{N_o}{2}, & |f| \le B \\ 0, & |f| > B \end{cases} \tag{3.1}$$

where B is the bandwidth of the signal, and $N_o B$ is the input power of $s(t)$. Since F-OFDM is a variation of OFDM [48], equation (3.1) can also be applied to F-OFDM signals.

As discussed in Chapter 2, the nonlinearity of RF amplifiers can be described by IP_3 or 1dB compression point. In [13], an explicit spectrum expression which is related to the out-band power emission levels of an RF amplifier and its IP_3 is developed. In many cases, 3rd-order IM distortion is dominant and other higher-order IM distortions are neglectable, and IP_3 is sufficient to describe the nonlinearity of RF amplifiers.

However, as the input power further increases, IP_3 only might be not enough to describe the spectrum regrowth when 5th-order IM appear and become relatively high compared to 3rd-order IM. [14] then expressed the output spectrum regrowth in terms of *G*, IP_3, and IP_5 of RF amplifiers.

Further increasing the power of input signal, higher- (beyond fifth-) order IM distortions will become non-neglectable because they now might be above the noise floor [15]. For estimating the higher-order spectrum regrowth, [16] proposed a general amplified spectrum model based on the *n*th-order IM products. Based on [16, eq. (31)], with (3.1), the final expression of the amplified spectrum (shifted to carrier frequency f_c) $P_{out}(f)$ up to arbitrary odd order ($2N-1, n \geq 1$) is

$$P_{\text{out}}(f) = \begin{cases} \sum_{n=1}^{N} \{ \frac{1}{(2n-1)!} \left| \sum_{l=0}^{N-n} \frac{(2l+2n-1)!}{2^l \cdot l!} \cdot a_{2l+2n-1} (P_s)^l \right|^2 \cdot \frac{1}{(2n-2)!} \frac{1}{B} \left(\frac{N_o B}{2} \right)^{2n-1} \\ \cdot \sum_{r=0}^{n-q} (-1)^r \binom{2n-1}{r} \left((2n-2r-1) - \frac{|f - f_c|}{B} \right)^{2n-2} \}, \\ \qquad \text{for } (2q-3)B \leq |f - f_c| < (2q-1)B, \quad 1 \leq q \leq n; \\ 0, \qquad \text{for } |f - f_c| > (2N-1)B. \end{cases} \tag{3.2}$$

where a_{2n-1} is the $(2n\text{-}1)^{\text{th}}$-order coefficient of Taylor series in (2.11). To solve the coefficients a_{2n-1} in (3.2), the authors in [16] firstly relates the output complex of $(2n\text{-}1)^{\text{th}}$-order IM products $\bar{A}_{2n-1}(t)$ to a_{2n-1} as

$$\bar{A}_{2n-1} = \sum_{i=n}^{N} \binom{2n-1}{n-i} \Big/ 4^{i-1} \cdot a_{2i-1} \cdot A^{2i-1} \tag{3.3}$$

where A is the amplitude of the input signal. In a two-tone test, $\bar{A}_{2n-1}(t)$ in (3.3) can be related to the output power of $(2n\text{-}1)^{\text{th}}$-order IM as [16, eq. (12)]

$$p_{IM,2n-1} = \frac{|\bar{A}_{2n-1}(t)|^2}{8R} \tag{3.4}$$

where $p_{IM,1}$ is the output power of passband, and $p_{IM,2n-1}$ (n = 2, 3, 4, …) are that of the $(2n\text{-}1)^{\text{th}}$-order IM products which can be measured via a two-tone test as shown in Figure 2.5. The unit of $p_{IM,2n-1}$ in (3.4) is Watts. The relation between $p_{IM,2n-1}$ in Watts and $P_{IM,2n-1}$ in dBm is

$$P_{IM,2n-1} = 10\log(p_{IM,2n-1}\cdot 10^3)\text{dBm} \tag{3.5}$$

With (3.2)-(3.5), one can predict the arbitrary order output spectrum regrowth based on the measured IM products via a two-tone test. Since the measurement of amplified OFDM output spectrum requires the spreading input signal that is generated from baseband, this method is much easier to measure IM products of a two-tone test than the amplified OFDM output spectrum. However, the Taylor coefficients used in the final spectrum expression (3.2) need to be solved in a set of equations which include $(2n\text{-}1)^{\text{th}}$-order IM products measurements. Thus, it is complicated to use. In addition, this approach for obtaining the output complex envelop of $(2n\text{-}1)^{\text{th}}$-order IM products includes extra terms of Taylor series coefficients on the right side of (3.3), which causes the result inaccurate.

In the next, several disadvantages of the spectrum model (3.2) will be discussed. And an explicit expression is proposed by relating an estimation of output spectrum of

a RF amplifier to its nonlinearity parameter, intercept points. At last, the presented analytical model is verified by experimental measurements.

3.2 Deriving the power spectrum density by using higher-order intercept points

In Figure 2.8, the blue line describes the output power at fundamental frequency vs. input power P_{in}, and the red line describe the power of $(2n\text{-}1)^{th}$-order IM product $P_{IM,2n-1}$ versus P_{in}. The point where the red line and the blue line intercept is defined as $(2n\text{-}1)^{th}$-order intercept point IP_{2n-1}. It is seen that as P_{in} increases, $P_{IM,2n-1}$ will increase accordingly. Therefore, a two-tone test will be needed repeatedly for measuring $P_{IM,2n-1}$ in (3.4) when P_{in} varies, which further increases the implement complexity of (3.2).

For calculating IP_{2n-1}, the two lines in Figure 2.8 should be determined first. For a specific RF amplifier at a given carrier frequency, the slope of the blue line (equals to 1) and the gain are known, the blue line then will be uniquely determined. Although the slope of the red line is known as $(2n\text{-}1)$, we need to determine one point $(P_{in}, P_{IM,2n-1})$ anywhere on this line. By choosing an input power P_{in} (in its effective input range) for the same condition, the corresponding $P_{IM,2n-1}$ can be obtained through a two-tone test. It is known that $P_{IM,2n-1}$ varies with P_{in}, the point $(P_{in}, P_{IM,2n-1})$ will always locate on the red line. With the slope $2n\text{-}1$ and the coordinate of this point, the red line now can be uniquely determined for the same RF amplifier at the same carrier frequency. Once the red line and the blue line are determined, the $(2n\text{-}1)^{th}$-order intercept point will be

uniquely determined even if input power level is adjusted. Therefore, for measuring intercept points of a RF amplifier as a specific carrier frequency, a two-tone test is needed only once. Therefore, we will replace $P_{IM,2n-1}$ by using intercept points below to simplify the implement complexity.

For calculating the Taylor coefficients a_{2n-1} in (3.2), the authors in [38] relate a_{2n-1} to IP_{2n-1} of RF amplifiers as equation (2.25). In (2.25), IP_{2n-1} can be calculated by using (2.21) via a two-tone test.

Substituting (2.28) into (3.2), $P_{out}(f)$ now can be derived as

$$P_{\text{out}}(f)=\begin{cases}\sum_{n=1}^{N}\{\frac{1}{(2n-1)!}|\sum_{l=0}^{N-n}\frac{(2l+2n-1)!}{2^l\cdot l!}\cdot[\frac{-2^{l+n-1}}{\binom{2l+2n-1}{l+n}}]\cdot 10^{[-(l+n-1)IP_{2l+2n-1}/10+(2l+2n-1)G/20]}(N_oB)^l|^2 \\ \cdot\left(\frac{1}{(2n-2)!}\frac{1}{B}\left(\frac{P_s}{2}\right)^{2n-1}\right)\cdot\left[\sum_{r=0}^{n-q}(-1)^r\binom{2n-1}{r}\left((2n-2r-1)-\frac{|f-f_c|}{B}\right)^{2n-2}\right]\}, \\ \qquad\qquad \text{for } (2q-3)B\le|f-f_c|<(2q-1)B,\quad 1\le q\le n; \\ 0, \\ \qquad\qquad \text{for } |f-f_c|>(2N-1)B.\end{cases} \tag{3.6}$$

From (3.6), a few observations are described as follows:

a. If the power of an input signal is given and a_{2n-1} is correctly calculated, the amplified output spectrum $P_{out}(f)$ can be predicted within $(2N\text{-}1)B$ frequency range. For example, the passband of an output signal is $|f-f_c|<B$

for $q=1$; the adjacent channel close to passband is $B<|f-f_c|<3B$ for $q=2$; and the next adjacent channel is $3B<|f-f_c|<5B$ for $q=3$.

b. The output spectrum in band $|f-f_c|>(2N-1)B$ is 0. The result is obtained because the input signal is assumed to be bandlimited in the derivation. In practical cases, no bandpass signal is exactly bandlimited within [-*B*, *B*], which indicates that in band $|f-f_c|>(2N-1)B$, the output spectrum is not exactly 0. However, the emission power most likely will be covered by noise in this band.

c. This spectrum model is explicit in terms of amplifier parameters, IP_{2n-1} and *G*, together with *B*, f_c, and input power, which makes the implementation of this model easily.

d. Intercept points are specific figures of merit, which are independent of input signal level. Thus, for same RF amplifiers at same carrier frequency, a two-tone test is needed only once for measuring the IP_{2n-1}, and IP_{2n-1} can be further used to calculate Taylor coefficients using. Since $p_{IM,2n-1}$ in (3.4) is dependent of input signal level, the users need to repeatedly conduct a two-tone test as the level of input signals varies for measuring $p_{IM,2n-1}$.

e. Due to the spectrum similarities of the FBMC modulation and F-OFDM [16] techniques, the derivation can be used to predict the power spectrum of amplified FBMC and F-OFDM signals.

3.3 Estimating Fifth-Order Intercept Point by Using 1dB Compression Point from Datasheets

In practice, the third-order IM distortions (i.e., $N = 2$ in (3.6)) are often dominant. In this case, equation (3.6) can estimate the power spectrum by using the IP_3 and gain only. Practically, before requesting RF amplifier samples for lab trials, datasheets are often the sole resource about the capability and characteristics, such as IP_3 and G, for preselecting RF amplifiers.

By further increasing the input power, 5th-order IM distortions (i.e. $N = 3$ in (3.6)) might be non-neglectable. Equation (3.6) now can estimate the output spectrum by using IP_3, IP_5 and G. But IP_5 is not always included in data sheets. To predict power spectrum with 5th-order IM distortions, a convenient method to first estimate IP_5 using output 1dB compression point with IP_3 from data sheets is discussed.

Based on [14] and [49], IP_5 can be derived in terms of fifth-order Taylor coefficients a_5 as

$$IP_5 = \frac{5G}{4} - 5\log\frac{5}{2}|a_5| \tag{3.7}$$

In [50], a_5 could be further estimated from input 1dB compression point $P_{1\text{dB\_in}}$, G, and IP_3 as

$$a_5 = 0.4\times 10^{[(3G/20)+(-P_{1\text{dB\_in}}/10)+(-IP_3/10)]} - 0.043\times 10^{(G-4P_{1\text{dB\_in}})/20} \tag{3.8}$$

where $P_{1\text{dB\_in}} = P_{1\text{dB\_out}} - G + 1$. Inserting (3.8) into (3.7), IP_5 now can be derived as

$$IP_5 = \frac{5}{4}G - 5\log_{10}\left|10^{[(3G/20)+(-P_{1\text{dB\_in}}/10)+(-IP_3/10)]} - 0.1075\times 10^{(G-4P_{1\text{dB\_in}})/20}\right| \tag{3.9}$$

To meet the ACPR or SEM wireless communication standards, appropriate RF amplifiers are needed for the RF systems. The spectrum model in (3.6) with $N = 3$ and (3.9) could help RF engineers reduce the number of candidates in pre-selection of RF amplifiers prior to the laboratory trials by using only data sheets, which provide IP_3, G and 1dB compression point.

3.4 Experimental Setup and Results

The proposed spectrum model was evaluated using the experimental setup described in Figure 3.1 It consists of one vector signal generator (Keysight ESG 4438C) as a wireless transmitter, one RF amplifier (Mini-Circuit ZFL-1000LN+) as the device under test, one DC power (Tektronix PS2520G) supply providing power for the RF amplifier for further algorithm verification, and a PC using MATLAB to plot the experimental results and the analytical prediction for comparison.

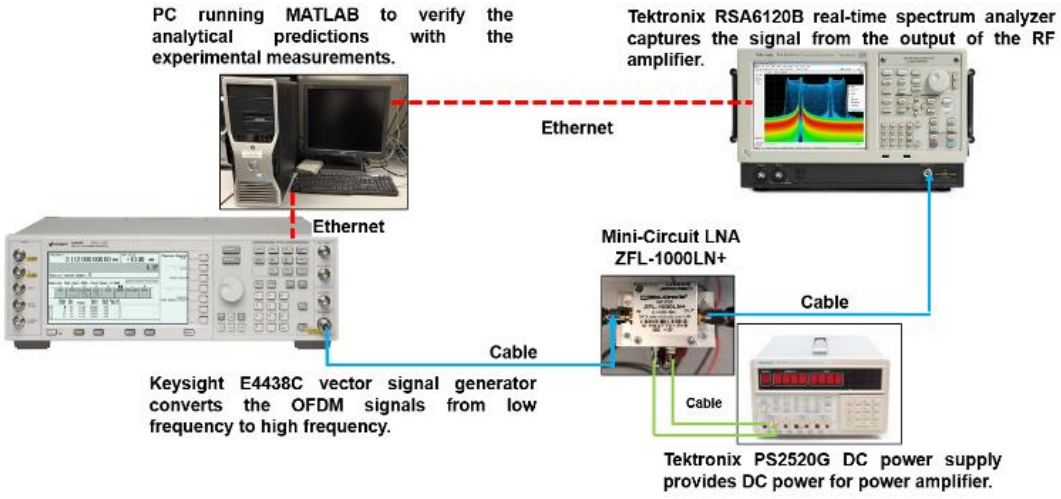

Figure 3.1. Experimental setup and RF amplifier under test.

ESG 4438C signal generator was set to transmit OFDM signals with a 5 MHz bandwidth at the carrier frequency of 880 MHz based on the standards of LTE operating bands [51]. The outputs from the signal generator were fed to the RF amplifier under test. The output signals of the RF amplifier were then captured by the Tektronix RSA 6120B spectrum analyzer, which were stored for further signal verification by a PC. Three different input scenarios are chosen as: the input power of scenario I is -20.8 dBm, the input power of scenario II is -15.8 dBm, and the input power of scenario III is -11.6 dBm.

To predict the OFDM output spectrum, we first measure the powers of IM from a two-tone test with two 875 MHz and 885 MHz carrier frequencies. As the input power is -16.8 dBm, the corresponding measured $P_{\mathrm{IM},\,1}$, $P_{\mathrm{IM},\,3}$, $P_{\mathrm{IM},\,5}$, and $P_{\mathrm{IM},\,7}$ of lower sideband are -10.96 dBm, -31.02 dBm, -56.66 dBm, and -63.9 dBm, and that of higher sideband are -10.98 dBm, -30.91 dBm, -56.93 dBm, and -64.24 dBm, respectively. It should be noticed that $P_{IM,\,2n-1}$ should be calculated as the average of the lower power of $(2n\text{-}1)^{\text{th}}$-order IM product $P_{IML,\,2n-1}$ and the higher power of $(2n\text{-}1)^{\text{th}}$-order IM product $P_{IMR,\,2n-1}$, which is

$$P_{IM,\,2n-1} = (P_{IML,\,2n-1} + P_{IMR,\,2n-1}) / 2 \tag{3.10}$$

Based on (3.10), IP_3, IP_5, and IP_7 at 880 MHz carrier frequency are calculated as 13.03 dBm, 14.49 dBm, and 11.88 dBm, respectively. After loading the stored output signals of these three scenarios, respectively, the measured output spectra and the

predicted output spectra are plotted together in Figure 3.2(a), Figure 3.2(b), and Figure 3.2(c).

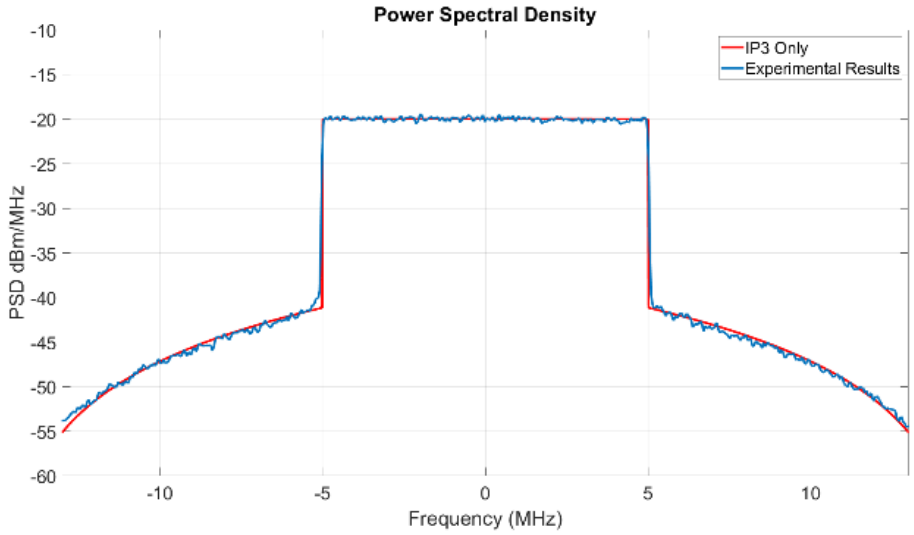

(a)

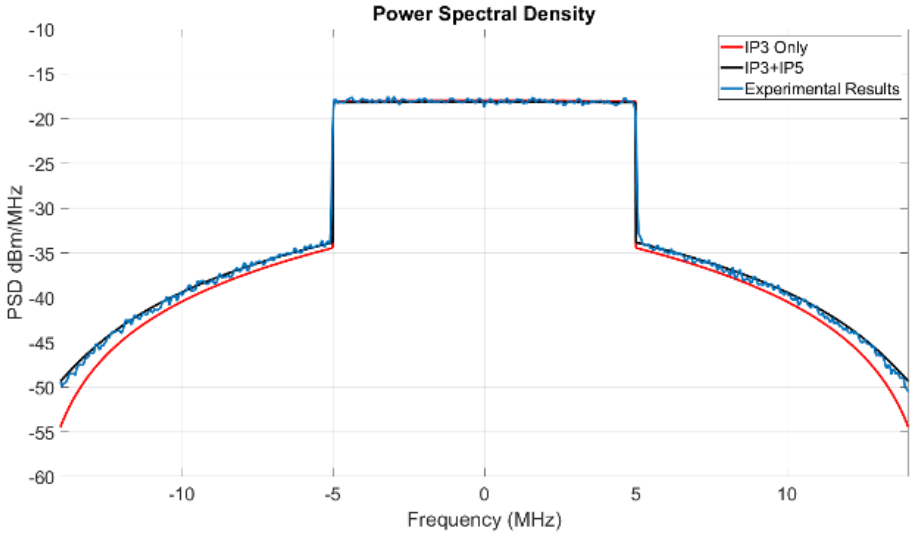

(b)

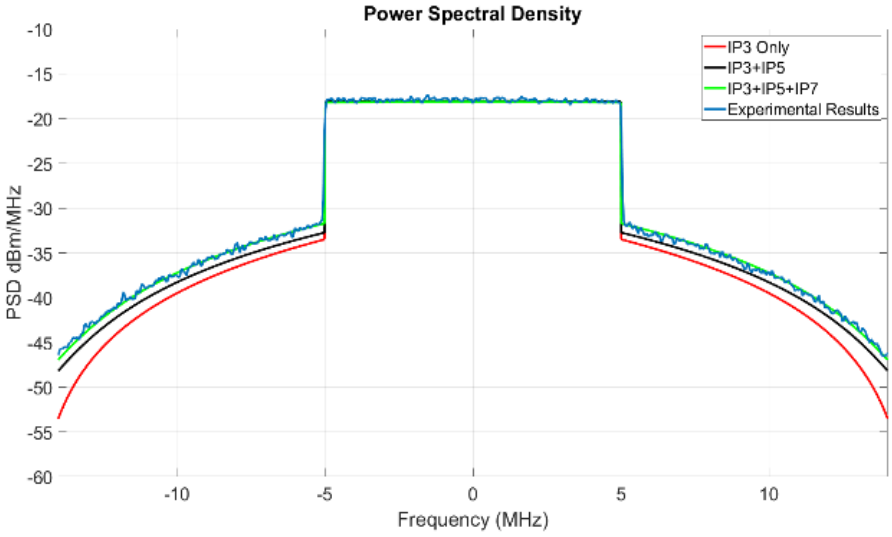

(c)

Figure 3.2. (a) Predicted output power spectrum considering IP_3 only for scenario I; (b) Predicted output power spectrum considering IP_3 and IP_5 vs IP_3 only for scenario II; (c) Comparison among predicted output spectrum of considering IP_7, IP_5, and IP_3, that of considering IP_3 only for scenario III.

In Figure 3.2(a) (scenario I), it is seen that the experimental measurement (blue waveform) well matches the theoretically predicted PSD using IP_3 (red line) only. In Figure 3.2 (b) (scenario II), as the input power is increased, IP_3 is not sufficient to describe the nonlinearity of RF amplifiers, and there are some misalignments in passband area between theoretical calculation including IP_3 only (red line) and experimental measurement (blue waveform). We can see that a better PSD fit exists when both IP_3 and IP_5 are used (black line) vs. IP_3 (red line) only. In Figure 3.2 (c) (scenario III), as the input power is further increased, the theoretic calculation with IP_3

and IP_5 (black line) is closer to experimental measurement (blue waveform) than that with IP_3 (red line) only, and the predicted spectrum with IP_7, IP_5, and IP_3 (green line) best matches the experimental measurement.

Table 3.1 Frequency Terms of Out-of-Band Intermodulation

Input Power (dBm)	Parameters	ACEPR (dB)
Scenario I: -20.8	IP_3 only	-38.921
Scenario II: -15.8	IP_3 only	-35.293
	IP_3 and IP_5	-39.794
Scenario III: -11.6	IP_3 only	-28.209
	IP_3 and IP_5	-32.985
	IP_3, IP_5 and IP_7	-40.608

In Table 3.1, the model for predicting the spectrum regrowth is evaluated by using the adjacent channel error power ratio (ACEPR), calculated as the difference between the measured and modelled signal, in the adjacent channel relative to the power within the passband [52]. The ACEPR is given by

$$\text{ACEPR} = 10\log\left(\frac{\int_{f_{adj}} |Y_{measured}(f) - Y_{model}(f)|^2 \, df}{\int_{f_{chan}} |Y_{measured}(f)|^2 \, df}\right) \tag{3.11}$$

where $Y(f)$ denotes the Fourier transform of the corresponding signal and f_{chan} and f_{adj} are the frequency bands of the carrier channel and the standard first (upper and lower) adjacent channels.

It is known that the lower ACEPR, the less misalignment exists. In scenario II, the ACEPR is decreased by 4.5 dB when both IP_3 and IP_5 are considered; In scenario III, the ACEPR is lowest wen IP_3, IP_5, and IP_7 are considered together. Therefore, further increasing the power of input signals, higher- (beyond seventh-) order distortions might be needed for prediction. Equation (3.6) provided is in general form, and the OFDM output spectrum can be predicted in any order.

Chapter 4 Improving the Measurements of IP_3

In chapter 3, based on Taylor polynomial coefficients, a power spectrum expression for amplified OFDM signals in terms of intercept points (up to n^{th}-order) is derived. Only the accurate P_t and $P_{IM,2n-1}$ are obtained from measurement, we could calculate the accurate intercept points such that predict the spectrum regrowth for the output signals. However, errors are existed in the measurements.

IP_3 is a very important figure of merit which gauges nonlinearity for RF amplifiers. Although IP_3 varies at different frequencies, it is worthy noticing that IP_3 may remain invariant at different input levels due to its definition as shown in Figure 2.7. Conventionally, IP_3 is calculated from the simultaneous measurement of the output power at fundamental tones and the 3^{rd}-order IM products via a two-tone test. However, the measured output power at fundamental frequencies is not only attributed to the linear amplification, but also attributed to 3^{rd}-order IM products. As the input signal further increases, the higher-order IM might be non-neglectable, which will directly impact the measurements at fundamental frequencies and to the lower IM products. A similar issue arises for the intercept points measurements beyond the 3^{rd}-order.

In this chapter, starting with a two-tone test, the impacts from 3^{rd}-order IM products to fundamental tones are analyzed. The measured IP_3 is thus corrected by removing the 3^{rd}-order IM impacts from fundamental tones. A description on improving intercept points of different orders using higher order is then discussed. IP_3 comparison between the result of the conventional method and that of the corrected method are analyzed lastly.

4.1 Improvements for IP_3 measurement using 3rd-order IM

In many cases, 3rd-order IM distortion is dominant and other higher-order IM distortions are neglectable, and IP_3 is sufficient to describe the nonlinearity of RF amplifiers. As shown in Figure 2.7, the output level of the fundamental frequency (f_{c1} or f_{c2}) rises at a rate of 1:1 with respect to the input power level, and that of third-order IM product ($2f_{c1} - f_{c2}$ or $2f_{c2} - f_{c1}$) will rise at a rate of 3:1 with respect to the input power level. Based upon ratios of these two straight lines [39]. IP_3 can be calculated as

$$IP_3 = \frac{(3P_t - P_{IM,3})}{2} \tag{4.1}$$

where P_t is the power at fundamental frequencies with linear amplification, and $P_{IM,3}$ is the power of 3rd-order IM products. Both of them can be measured simultaneously in a two-tone test. With the linear amplification, the amplitude of one of two output fundamental tones is $a_1 A$, and the linear output power P_t can be expressed by using (2.15) as

$$P_t = 10 \times \log[(\frac{a_1 A}{\sqrt{2}})^2 \frac{10^3}{R}] \quad \text{dBm} \tag{4.2}$$

Due to the broad dynamic range of the signals involved in RF amplifier, power quantities are usually expressed in logarithmic units [17].

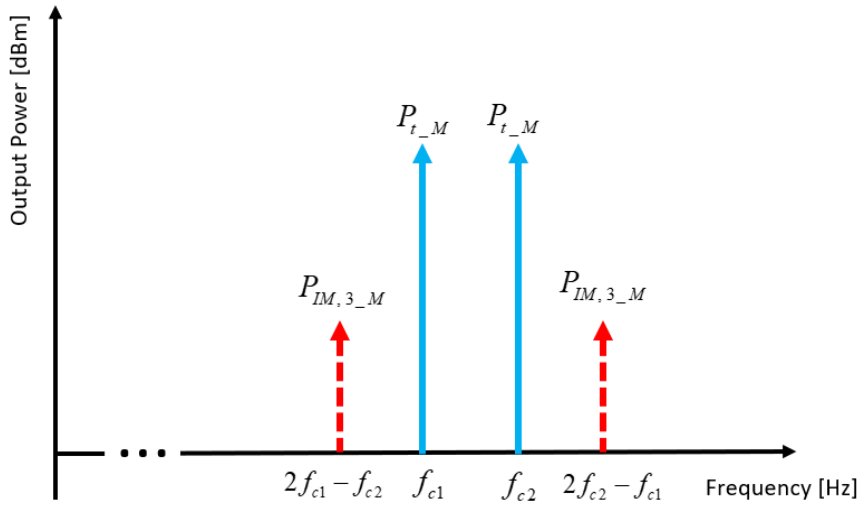

Figure 4.1. A two-tone test considering 3rd-order IM products only.

Conventionally, P_t and $P_{IM,3}$ are measured directly at those frequencies which are illustrated in Figure 4.1, via a two-tone test. However, the measured output power at fundamental frequencies P_{t_M} actually includes nonlinear effects generated by 3rd-order IM products, which leads to $P_{t\_M} \neq P_t$ as proved next. Thus, the amplified power at fundamental frequency will compress, which is described by the blue solid curve as shown in Figure 4.2. For calculating IP_3, P_t need to be corrected by removing the 3rd-order effects from P_{t_M} before using (4.1).

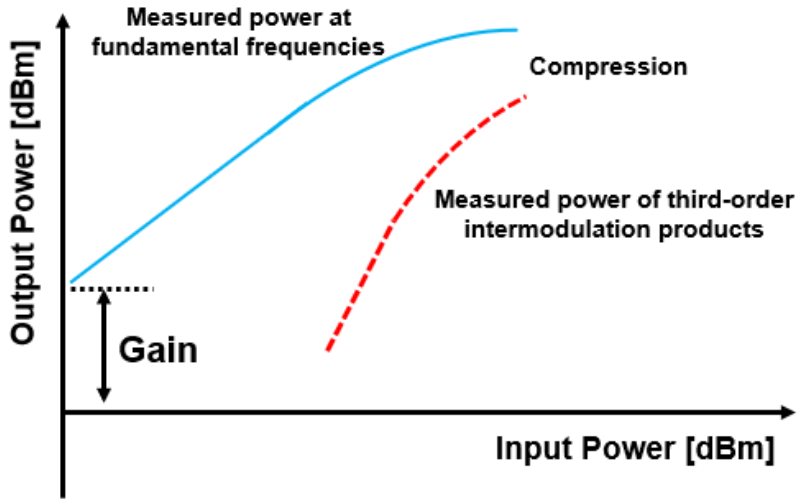

Figure 4.2. Blue solid curve denotes the measured power at fundamental frequencies versus input power, and the red dash curve denotes the measured power of 3rd-order IM products versus input power.

In a two-tone test, considering 3rd-order nonlinear distortions only, equation (2.21) can be expressed as

$$\begin{aligned} y(t) &= b_1(\cos 2\pi f_1 t + \cos 2\pi f_2 t) \\ &\quad + b_3[\cos(4\pi f_1 - 2\pi f_2)t + \cos(4\pi f_2 - 2\pi f_1)t] \end{aligned} \tag{4.3}$$

where

$$b_1 = a_1 A + \frac{9}{4} a_3 A^3 \tag{4.4}$$

$$b_3 = \frac{3}{4} a_3 A^3 \tag{4.5}$$

The measured output power at fundamental frequencies P_{t_M} and that of the 3rd-order IM products $P_{IM,3\_M}$ can be derived respectively as

$$\begin{aligned} P_{t\_M} &= 10\times\log[(\frac{b_1}{\sqrt{2}})^2\frac{10^3}{R}]\ \text{dBm} \\ &= 10\times\log[(\frac{a_1A+\frac{9}{4}a_3A^3}{\sqrt{2}})^2\frac{10^3}{R}]\ \text{dBm} \end{aligned} \tag{4.6}$$

$$\begin{aligned} P_{IM,3\_M} &= 10\times\log[(\frac{b_3}{\sqrt{2}})^2\frac{10^3}{R}]\ \text{dBm} \\ &= 10\times\log[(\frac{\frac{3}{4}a_3A^3}{\sqrt{2}})^2\frac{10^3}{R}]\ \text{dBm} \end{aligned} \tag{4.7}$$

Based on (4.5) and (4.7), it is noted that $P_{IM,3\_M}$ contains the 3rd-order distortion before 5th-order IM products appear when the input power increases (even though the high-order IM products are neglectable) such that $P_{IM,3\_M}$ equals to $P_{IM,3}$, and $P_{IM,3\_M}$ is in the linear region of the red dash curve in Figure 4.2. Thus, $P_{IM,3\_M}$ can be used directly in (4.1) for calculation. But with (4.4) and (4.6), it is noticed that the measured amplitude of the output at fundamental frequencies is $(a_1A+\frac{9}{4}a_3A^3)$ instead of linear amplification a_1A only, which indicates that P_{t_M} cannot be used directly in (4.1). Therefore, to obtain the P_t, the 3rd-order effects need to be removed from P_{t_M}.

According to (4.6), the linear amplified amplitude a_1A in (4.2) can be derived as

$$a_1 A = \sqrt{2R \cdot 10^{\frac{P_{t\_M}}{10}-3}} - \frac{9}{4} a_3 A^3 \tag{4.8}$$

For determine $a_1 A$, the term $\frac{9}{4} a_3 A^3$ in (4.8) need to be calculated. From (4.7), $\frac{9}{4} a_3 A^3$ can then be derived as

$$\frac{9}{4} a_3 A^3 = \pm 3\sqrt{2R \cdot 10^{\frac{P_{IM,3\_M}}{10}-3}} \tag{4.9}$$

As shown in the blue solid line of Figure 4.2, the amplified power at fundamental frequency will saturate beyond a certain value of the input power such that a_3 should be negative for the gain compression in (4.9). Thus, $\frac{9}{4} a_3 A^3$ is

$$\frac{9}{4} a_3 A^3 = -3\sqrt{2R \cdot 10^{\frac{P_{IM,3\_M}}{10}-3}} \tag{4.10}$$

With (4.2), (4.8) and (4.10), P_t can be corrected from P_{t_M} as

$$\begin{aligned} P_{t\_\text{corr}} &= 10 \times \log[(\frac{\sqrt{2R \cdot 10^{\frac{P_{t\_M}}{10}-3}} + 3\sqrt{2R \cdot 10^{\frac{P_{IM,3\_M}}{10}-3}}}{\sqrt{2}})^2 \frac{10^3}{R}] \text{ dBm} \\ &= 10 \times \log[(\sqrt{10^{\frac{P_{t\_M}}{10}-3}} + 3\sqrt{10^{\frac{P_{IM,3\_M}}{10}-3}})^2 10^3] \text{ dBm} \end{aligned} \tag{4.11}$$

Substituting (4.11) into (4.1), we can get the corrected IP_3 as

$$\begin{aligned} \overline{IP_3} &= \frac{(3P_{t\_\text{corr}} - P_{IM,3\_M})}{2} \\ &= \frac{30\log[(\sqrt{10^{\frac{P_{t\_M}}{10}-3}} + 3\sqrt{10^{\frac{P_{IM,3\_M}}{10}-3}})^2 10^3] - P_{IM,3\_M}}{2} \end{aligned} \tag{4.12}$$

The error ε between $\overline{IP_3}$ and IP_3 without corrections IP_{3_M} can further be calculated as

$$\begin{aligned}\varepsilon &= \overline{IP_3} - IP_{3\_M} \\ &= \frac{(3P_{t\_\mathrm{corr}} - P_{IM,3\_M})}{2} - \frac{(3P_{t\_M} - P_{IM,3\_M})}{2} \\ &= \frac{3}{2}10\log[(1+3\sqrt{10^{\frac{P_{IM3\_M}-P_{t\_M}}{10}}})^2]\end{aligned} \tag{4.13}$$

4.2 Improvement of intercept points from higher-order IM measurements

As the input power increases, assuming 5th-order IM distortion will become non-neglectable such that IP_5 might be needed for quantifying the nonlinearity, before considering higher-order (beyond 5th-order) IM distortions. Based on [39], IP_5 can be calculated as

$$IP_5 = \frac{5P_t - P_{IM,5}}{4} \tag{4.14}$$

where $P_{IM,5}$ is the power of 5th-order IM products. P_t, $P_{IM,3}$, and $P_{IM,5}$ now can be measured directly via a two-tone test at those frequencies which is illustrated in Figure 2.3. However, the measured output power at fundamental frequencies P_{t_M} includes the nonlinear effects from 3rd-order IM products and 5th-order IM products, which leads to $P_{t\_M} \neq P_t$, and the measured $P_{IM,3\_M}$ now includes the nonlinear effects from 5th-order IM products, which leads to $P_{IM,3} \neq P_{IM,3\_M}$. Before calculating IP_5 via (4.14), P_t needs to be determined correctly.

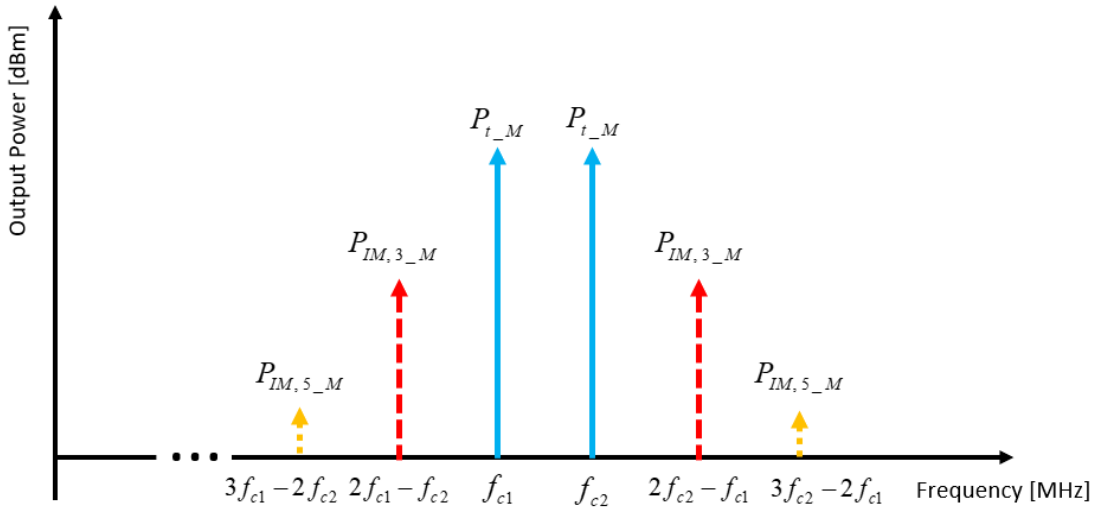

Figure 4.3. A two-tone test considering 3rd-order and 5th-order IM products.

In this case, if other products that locate far away from the two fundamental tones are filtered out, equation (2.21) now is written as

$$\begin{aligned} y(t) &= b_1(\cos\omega_1 t + \cos\omega_2 t) \\ &+ b_3[\cos(2\omega_1 - \omega_2)t + \cos(\omega_2 - \omega_1)t] \\ &+ b_5[\cos(3\omega_1 - 2\omega_2)t + \cos(3\omega_2 - 2\omega_1)t] \end{aligned} \tag{4.15}$$

where

$$b_1 = a_1 A + \frac{9}{4}a_3 A^3 + \frac{25}{4}a_5 A^5 \tag{4.16}$$

$$b_3 = \frac{3}{4}a_3 A^3 + \frac{25}{8}a_5 A^5 \tag{4.17}$$

$$b_5 = \frac{5}{8}a_5 A^5 \tag{4.18}$$

Due to 5th-order IM products become visible, from (4.14), it is noticed that the output amplitude at fundamental frequencies now become $(a_1 A + \frac{9}{4}a_3 A^3 + \frac{25}{4}a_5 A^5)$,

and output amplitude of the 3rd-order IM products now become $(\frac{3}{4}a_3A^3+\frac{25}{8}a_5A^5)$. Thus, it is known that the 5th-order IM now not only have an impact directly on fundamental frequencies, but also on 3rd-order IM products. In this situation, if IP_5 is going to be calculated, only P_{t_M} needs to be corrected; but if IP_3 is going to be calculated, both P_{t_M} and $P_{IM,3\_M}$ are needed to be corrected simultaneously.

The measured output power at fundamental frequencies P_{t_M}, that of the 3rd-order IM products $P_{IM,3\_M}$, and that of the 5th-order IM products $P_{IM,5\_M}$ can be derived using (4.16)-(4.18) respectively as

$$\begin{aligned} P_{t\_M} &= 10\times\log[(\frac{b_1}{\sqrt{2}})^2\frac{10^3}{R}]\ \text{dBm} \\ &= 10\times\log[(\frac{a_1A+\frac{9}{4}a_3A^3+\frac{25}{4}a_5A^5}{\sqrt{2}})^2\frac{10^3}{R}]\ \text{dBm} \end{aligned} \tag{4.19}$$

$$\begin{aligned} P_{IM,3\_M} &= 10\times\log[(\frac{b_3}{\sqrt{2}})^2\frac{10^3}{R}]\ \text{dBm} \\ &= 10\times\log[(\frac{\frac{3}{4}a_3A^3+\frac{25}{8}a_5A^5}{\sqrt{2}})^2\frac{10^3}{R}]\ \text{dBm} \end{aligned} \tag{4.20}$$

$$\begin{aligned} P_{IM,5\_M} &= 10\times\log[(\frac{b_3}{\sqrt{2}})^2\frac{10^3}{R}]\ \text{dBm} \\ &= 10\times\log[(\frac{\frac{5}{8}a_5A^5}{\sqrt{2}})^2\frac{10^3}{R}]\ \text{dBm} \end{aligned} \tag{4.21}$$

From (4.16) and (4.19), it is noted that P_{t_M} is attributed to linear amplification, 3rd-order effects and 5th-order effects, and $P_{IM,3\_M}$ is attributed to 3rd-order effects and

5th-order effects. To obtain P_t, the 3rd-order effects and 5th-order effects need to be removed from P_{t_M}. In this case, the linear amplified amplitude $a_1 A$ can be derived from (4.19) as

$$a_1 A = \sqrt{2R \cdot 10^{\frac{P_{t\_M}}{10}-3}} - \frac{9}{4} a_3 A^3 - \frac{25}{4} a_5 A^5 \tag{4.22}$$

The last term $\frac{25}{4} a_5 A^5$ in (4.22) is derived from (4.21) as

$$\frac{25}{4} a_5 A^5 = \pm 10\sqrt{2R \cdot 10^{\frac{P_{IM,5\_M}}{10}-3}} \tag{4.23}$$

As shown in the red dash curve of Figure 4.2, the power of 3rd-order IM products will saturate beyond a certain value of the input power. Thus, a_3 and a_5 should have opposite signs for 3rd-order IM compression. Since a_3 is negative, a_5 should be positive in (4.23). Thus, equation (4.23) can be written as

$$\frac{25}{4} a_5 A^5 = 10\sqrt{2R \cdot 10^{\frac{P_{IM,5\_M}}{10}-3}} \tag{4.24}$$

With (4.20) and (4.24), the term $\frac{9}{4} a_3 A^3$ in (4.22) is derived as

$$\frac{9}{4} a_3 A^3 = -3\sqrt{2R \cdot 10^{\frac{P_{IM,3\_M}}{10}-3}} - 15\sqrt{2R \cdot 10^{\frac{P_{IM,5\_M}}{10}-3}} \tag{4.25}$$

Combining (4.2), (4.22), (4.24), and (4.25), P_t can be corrected as

$$P_{t\_\mathrm{corr}} = 10\log[(\sqrt{10^{\frac{P_{t\_M}}{10}-3}} + 3\sqrt{10^{\frac{P_{IM,3\_M}}{10}-3}} + 5\sqrt{10^{\frac{P_{IM,5\_M}}{10}-3}})^2 10^3]\ \mathrm{dBm} \tag{4.26}$$

With (4.14), (4.24) and (4.26), we can get the corrected IP_5 as

$$\overline{IP_5} = \frac{(5P_{t\_\mathrm{corr}} - P_{IM,5\_M})}{4} = \frac{50\log[(\sqrt{10^{\frac{P_{t\_M}}{10}-3}} + 3\sqrt{10^{\frac{P_{IM,3\_M}}{10}-3}} + 5\sqrt{10^{\frac{P_{IM,5\_M}}{10}-3}})^2 10^3] - P_{IM,5\_M}}{4} \quad (4.27)$$

For further improving IP_3 when 5th-order IM products become visible, $P_{IM,3}$ now need to be corrected with (4.20), (4.24) and (4.25) by removing the impacts from 5th-order IM products as

$$P_{IM,3\_\mathrm{corr}} = 10\log[(\sqrt{10^{\frac{P_{IM,3\_M}}{10}-3}} + 5\sqrt{10^{\frac{P_{IM,5\_M}}{10}-3}})^2 10^3] \text{ dBm} \quad (4.28)$$

Substituting (4.28) and (4.26) into (4.1), we can get the corrected IP_3 as

$$\overline{IP_3} = \frac{(3P_{t\_\mathrm{corr}} - P_{IM,3\_\mathrm{corr}})}{2} = \frac{30\log[(\sqrt{10^{\frac{P_{t\_M}}{10}-3}} + 3\sqrt{10^{\frac{P_{IM,3\_M}}{10}-3}} + 5\sqrt{10^{\frac{P_{IM,5\_M}}{10}-3}})^2 10^3]}{2} - \frac{10\log[(\sqrt{10^{\frac{P_{IM,3\_M}}{10}-3}} + 5\sqrt{10^{\frac{P_{IM,5\_M}}{10}-3}})^2 10^3]}{2} \quad (4.29)$$

The $(2n\text{-}1)^{\text{th}}$-order intercept point is calculated by [39]

$$IP_{2n-1} = \frac{(2n-1)P_t - P_{IM,2n-1}}{2n-2} \quad (4.30)$$

where $P_{IM,2n-1}$ is the power of the $(2n\text{-}1)^{\text{th}}$-order IM products. Similar improvements from the previous derivation could be extended to higher-order intercept point corrections.

Since in most cases, higher-order IM products are far less than 3rd-order IM products, they are often neglected. Thus, higher-order intercept points are of less

importance, evidenced by the unique availability of IP_3 from datasheets. Also, IP_3 should be measured before 5^{th}-order IM products appear.

Therefore, equation (4.11) is sufficient to correct IP_3 measurement. This is a simple yet significant improvement, hence is a practical and effective correction to use in testing. Also, equation (4.12) quantifies the error corrected in dB scale. We will use them in our experiment, as described next.

4.3 Experimental Measurements

To verify our hypothesis for correcting IP_3 measurements, a two-tone test with two 875 MHz and 885 MHz carriers was designed with the experiment setup as shown in Figure 3.1. For calculating IP_3, P_{t_M} and $P_{IM,3\_M}$ were obtained from the two-tone test as the input power increased from -28.6 dBm, to -21.8 dBm by using (3.10).

In Figure 4.4, the blue dot line denotes the IP_3 without correction versus input power, the red solid line denotes the corrected IP_3 versus input power, and the yellow dash line denotes the error between IP_3 with and without correction. It could be easily observed that, as the input power increases, the IP_3 without correction decreases, the error between these two lines increases. With the proposed correction method, the corrected IP_3 is flatter than that without correction, and its values are around 14.2 dBm which is close to 14 dBm given in datasheet. When the input power is -21.8 dBm, the error is over 1 dB, which is noticeable, such that the correction may become meaningful.

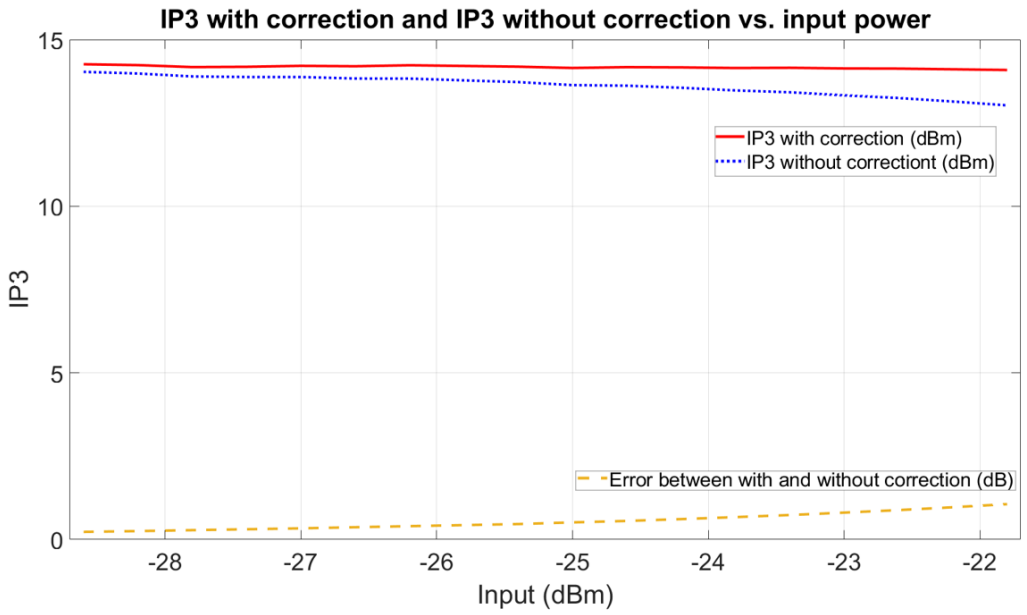

Figure 4.4. IP_3 with correction and IP_3 without correction versus input power.

As described in Figure 2.7, for an RF amplifier, IP_3 is defined to be a constant at a given frequency, independent from the input power variation. But when we directly use the output data without correction, IP_3 measurements obtained would be different, decreasing as the input power increases, which is shown in Figure 4.4 (blue dot line). With the correction, the measured IP_3 remains nearly flat in Figure 4.4 (red solid line).

Although P_t could be measured in the linear region before the 3rd-order IM products appear, but the low input power often results in high noise corruption. Practically, for IP_3 measurement, the P_t and $P_{IM,3}$ are measured at the same time. In the presence of the 3rd-order IM products, this corrective method provides a stable measuring range of input levels for calculating IP_3 as shown in Figure 4.4. Although

(4.25) provide the method to further correct IP_3, it is unnecessary as IP_3 could be well determined by (4.11) before 5^{th}- and higher- order IM products become visible.

Chapter 5 Conclusion and Future Work

In this dissertation, a spectrum model of RF amplifiers without memory effects is developed in terms of intercept points. Then, a simple but significant corrective method for measuring IP_3 by removing corresponding nonlinear impacts of 3^{rd}-order IM products from fundamental two tones is proposed. All the expressions are validated by experimental measurements.

5.1 Contributions

The main contributions of this dissertation are concluded in the following subsections as:

5.1.1 Predicting the power spectrum using higher-order intercept points

OFDM has been developed into a popular modulation scheme for wireless communication systems, used in applications such as LTE and 5G. In wireless communication systems, spectrum regrowth caused by RF amplifiers will generate distortions to both passband and adjacent channels such that the transmission quality is degraded. Due to the nonlinearity of RF amplifier, the model for predicting the spectrum regrowth of OFDM based output signals is studied.

Based on Taylor polynomial coefficients, a power spectrum expression for amplified OFDM signals in terms of intercept points (up to n^{th}-order) is derived. This model is useful to RF engineers in choosing and testing RF amplifiers with appropriate specifications, such as intercept points and gain, to meet the requirements of wireless standards. Measurements are carried out to confirm the results of the proposed model.

5.1.2 Correcting IP_3 measurements

IP_3 is an important parameter of RF amplifiers, and it is conventionally available from industrial datasheets. IP_3 can be utilized to estimate ACPR which is useful for RF amplifier design and testing in compliance with 5G standards. Also, it is the key parameter for predicting spectrum regrowth by using the proposed spectrum model in chapter 3.

Therefore, an accurate IP_3 measurement is of importance. IP_3 is often calculated from the interception between the line of the output power at fundamental frequencies versus the input power and the line of the power of the 3^{rd}-order intermodulation product measured from a two-tone test. However, the measured output power at fundamental frequency is not only from the fundamental tones, but is also affected by 3^{rd}-order IM products. Therefore, the impacts from 3^{rd}-order IM products to the fundamental tones are analyzed. As a solution, simple formulas that remove corresponding nonlinear effects are derived.

5.2 Future research topics

The following areas should be further pursed:

1. Extending this spectrum model by considering AM-PM nonlinear distortions.
2. Extending this spectrum model by considering memory effects.
3. Extending the proposed spectrum model on Massive MIMO systems.
4. Improving the intercept points measurements for other nonlinear components in transceivers, such as a mixer.

References

[1] W. Y. Chen, *DSL: Simulation techniques and standards development for digital subscriber line systems*. Indianapolis, IN, USA: Macmillan Tech., 1998.

[2] T. Starr, J. M. Cioffi, and P. Silverman, *Understanding digital subscriber line technology*. Upper Saddle River, NJ, USA: Prentice Hall, 1999.

[3] B. Farhang-Boroujeny and H. Moradi, "OFDM inspired waveforms for 5G," *IEEE Commun. Surveys Tuts.*, vol. 18, no. 4, pp. 2474-2492, 4th Quart., 2016.

[4] R. van Nee and R. Prasad, *OFDM for wireless multimedia communications*, Artech House, Boston, 2000.

[5] A. Tusha, S. Doğan, and H. Arsian, "A hybrid downlink NOMA with OFDM and OFDM-IM for beyond 5G wireless networks," *IEEE Signal Process. Lett.*, vol. 27, pp. 491-495, 2020.

[6] H. Shaiek, R. Zayani, Y. Medjahdi, and D. Roviras, "Analytical analysis of SER for beyond 5G post-OFDM waveforms in presence of high-power amplifiers," *IEEE Access*, vol. 7, pp. 29441-29452, 2019.

[7] H. Kim et al., "A 28-GHz COMS direct conversion transceiver with packaged 2×4 antenna array for 5G cellular systems," *IEEE J. Solid-State Circuits*, vol. 53, no. 5, pp. 1245-1259, May 2018.

[8] Y.S. Yeh, E. Balboni, and B. Floyd, "A 28-GHz phased-array transceiver with series-fed dual-vector distributed beamforming," in *Proc. IEEE Radio Freq. Intergr. Circuits Symp. (RFIC)*, Jun. 2017, pp. 65-68.

[9] J.D. Dunworth *et al.*, "A 28-GHz bulk-CMOS dual-polarization phased array transceiver with 24 channels for 5G user and basestation equipment," in *IEEE ISSCC Dig. Tech. Papers*, Feb. 2018, pp. 70-72.

[10] W. Lee, and S. Hone, "28 GHz RF Front-End Structure Using CG LNA as a Switch," *IEEE Microw. Wireless Compon. Lett.*, vol. 30, no. 1, Jan. 2020.

[11] C. Chang, and M. Onabajo, "Analysis and demonstration of an IIP3 Improvement Technique for low-power RF low-noise amplifiers," IEEE Trans. Circuits-I, vol. 65, no. 3, March 2018.

[12] C. Cho, W. W. Eisenstadl, B. Stengel and E. Ferrer, "IIP3 estimation from the gain compression curve," *IEEE Trans. Microw. Theory Tech.*, Vol. 53, No. 4, pp. 1197-1202, 2005.

[13] Q. Wu, M. Testa, and R. Larkin, "On design of linear RF power amplifier for CDMA signals," *Int. J. RF Microw. Comput. -Aided Eng.*, vol. 8, no. 4, pp.283-292, 1998.

[14] Q. Wu, H. Xiao and Li F., "Linear RF power amplifier design for CDMA signals: A spectrum analysis approach," *Microw. J.*, Vol. 41, No. 12, pp. 22-40, 1998.

[15] H. AI-Raweshidy and S. Komaki, *Radio over fiber technologies for mobile communications networks*. Norwood, MA, USA: Artech House, 2002.

[16] S. Yi, S. Nam, S. Oh and J. Han, "Prediction of a CDMA output spectrum based on intermodulation products of two-tone test," *IEEE Trans. Microw. Theory Tech.*, Vol. 49, No. 5, pp. 938-946, 2001.

[17] P. Colantonio, F. Giannini, and E. Limiti, *High efficiency RF and microwave solid state power amplifiers*. Chichester, UK: John Wiley and Sons, 2009.

[18] N. B. Carvalho, and J. C. Pedro, "Compact formulars to relate ACPR and NPR to two-tone IMR and IP3," Microw. J., vol. 42, no. 12, 1999.

[19] B. Schweber, *Understanding the basics of low-noise and power amplifiers in wireless designs*, 2013. Available online: https://www.digikey.com/en/articles/understanding-the-basics-of-low-noise-and-power-amplifiers-in-wireless-designs. (access on 6/25/20).

[20] C. Browick, *What's in RF front end?*, 2008. Available online: https://www.eetimes.com/whats-in-an-rf-front-end/ (access on 6/25/20).

[21] *Efficiency of microwave devices*. Available online: https://www.microwaves101.com/encyclopedias/efficiency-of-microwave-devices (access on 6/26/20).

[22] I. Rosu. Available online: http://www.qsl.net/va3iul/RF%20Power%20Amplifiers/RF_Power_Amplifiers.pdf. (access on 6/26/20).

[23] J. Browne, "Learn the meaning of amplifier linearity," *Microwaves & RF*, 2018. Available online: https://www.mwrf.com/technologies/components/article/21846558/learn-the-meaning-of-amplifier-linearity (access on 6/26/20).

[24] S. Cripps, *RF power amplifiers for wireless communications*. Norwood, MA, USA: Artech House, 1999.

[25] G. Doudorov, Evaluation of Si-LDMOS transistor for RF power amplifier in 2-6 GHz frequency range, Master Thesis, Linkoping University, Sweden, 2003.

[26] N. Pothecary, *Feedforward linear power amplifier*. Norwood, MA, USA: Artech House, 1999.

[27] S. Cripps, *Advanced techniques in RF power amplifier design*. Norwood, MA, USA: Artech House, 2002.

[28] P. Keningon, *High linearity RF amplifier design*. Norwood, MA, USA: Artech House, 2000.

[29] A. Ahmed, Analysis, modeling and linearization of nonlinearity and memory effects in power amplifiers used for microwave and mobile communications. PhD dissertation, Kassel University, Mar 2005.

[30] M. Kazimierczuk, *RF power amplifiers*. West Sussex, United Kingdom: John Wiley & Sons Ltd., 2008.

[31] J. Pedro, J. Madaleno and J. Garcia, "Theoretical basis for the extraction of mildly nonlinear behavioral models," *Int. J. RF and Microw. CAE*, vol. 13, no. 1, pp. 40-53, 2003.

[32] D. Schruers, M. O'droma, A. A. Goacher, and M. Gadringer, *RF power amplifier behavioral modeling*. Cambridge, UK: Cambridge University Press, 2009.

[33] F. Mkadem and S. Boumaiza, "Physically Inspired Neural Network Model for RF Power Amplifier Behavioral Modeling and Digital Predistortion," *IEEE Trans. Microw. Theory Tech.*, vol. 59, no. 4, pp. 913-923, 2011.

[34] L. W. Couch, *Digital and Analog Communication Systems*, 8th ed. Upper Saddle River, NJ, USA: Pretice-Hall, 2018.

[35] J. Golio, *The RF and microwave handbook*. Boca Raton, FL, USA: CRC Press, 2001.

[36] S. Amin, W. Van More, P. Händel, and D. Rönnow, "Characterization of concurrent dual-band power amplifiers using a dual two-tone excitation signal," IEEE Trans. Instrum. Meas., vol. 64, no.10, pp. 2781-2791, Oct. 2015.

[37] F.M. Gannouchi, H. Wakana, and M. Tanaka, "A new unequal three-tone signal method for AM-AM and AM-PM distortion measurements suitable for characterization of satellite communication transmitters/transponders," *IEEE Trans. Microw. Theory Tech.*, vol. 48, no. 8, 2000, pp. 1404-1407.

[38] Application notes, *Network analyzer measurements: filter and amplifier examples*, Agilent Technologies, 1997. Available online: https://www.keysight.com/us/en/assets/7018-06803/application-notes/5965-7710.pdf (access on 11/10/20).

[39] J. C. Pedro, and N. B. Carvalho, *Intermodulation distortion in microwave and wireless circuits*. Boston, USA: Artech House, 2003.

[40] X. Li, Nonlinearity analysis and predistortion of 4G wireless communication systems, Ph.D. dissertation, Portland State University, 2013.

[41] X. Li, C.M. Liu, Y. Xu, and F. Li, "Obtaining polynomial coefficients from intercept points of RF power amplifiers," *Electronics Lett.*, vol. 48, no. 19, pp. 1238-1240, 2012.

[42] Z. Ankarali, B. Pekoz, and H. Arslan, “Flexible radio access beyond 5G: A future projection on waveform, numerology, and frame design principles flex,” *IEEE Access*, vol. 5, pp. 18295-18309, 2017.

[43] L. Zhang, A. Ijaz, P. Xiao, and M. Molu, “Filtered OFDM systems, algorithms, and performance analysis for 5G and beyond,” IEEE Trans. Commun., vol. 66, no.3, pp. 1768-1782, 2017.

[44] R. Nissel, S. Schwarz, and H. Moradi, “Filter bank multicarrier modulation schemes for future mobile communications,” *IEEE J. Sel. Areas Commun.*, vol. 66, no. 8, pp. 1205-1218, 2017.

[45] M. Rajabzadeh, and H. Steendam, “Power spectral analysis of UW-OFDM systems,” *IEEE Trans. Commun.*, vol. 66, no. 6, pp. 2685-2695, 2018.

[46] X. Li, K. Tam, and F. Li, “Statistical model of OFDM and its application in nonlinearity analysis of LTE-advanced systems,” *Int. J. Electron. Lett., vol. 4, no. 3*, pp. 296-301, May 2015.

[47] S. Yan, X. Yang, X. Li, and F. Li, “A statistical model of FBMC-OQAM signals for predicting spectral regrowth,” *Int. J. Electron. Lett.*, 2020, doi:10.1080/21681724.2020.1734865.

[48] X. Yang, S. Yan, X. Li, and F. Li, “A unified spectrum formulation for OFDM, FBMC, and F-OFDM,” *Electronics*, vol. 9, no. 8, 2020.

[49] H. Xiao, Spectrum modelling for linear RF power amplifier design for digital cellular communication signals, Ph.D. dissertation, Portland State University, US, 1999.

[50] H. Al-Kanan, X. Yang, and F. Li, “Improved estimation for Saleh model and predistortion of power amplifier using 1-dB compression point,” J. Eng., vol. 2020, no. 1, pp. 13-18, 2020.

[51] Signal research group, *The LTE standard*, 2014. Available online: https://www.qualcomm.com/media/documents/files/the-ltestandard.pdf (access on 15/6/19).

[52] D. Schreus, M. O’Droma, A. A. Goacherm, and M. Gadringer, *RF power amplifier behavioral modeling*. New York, NY, USA: Cambridge Univ. Press, 2009.

Appendix

Clarification of the errors in equation (3.3) by using the derivation of 3rd-order two-tone test

As mentioned in Section 2.2, the two-tone input signal can be expressed as

$$s(t) = A \cdot \cos \omega_1 t + A \cdot \cos \omega_2 t \tag{A.1}$$

Substituting (A.1) into (2.12) and assuming n = 2, the output signal can be expressed as

$$\begin{aligned}
&x_{out}(t) = a_1 x_{in}(t) + a_3 x_{in}^3(t) \\
&= a_1 A(\cos \omega_1 t + \cos \omega_2 t) + a_3 A^3 (\cos \omega_1 t + \cos \omega_2 t)^3 \\
&= (a_1 A + \frac{9}{4} a_3 A^3) \cos \omega_{c1} t + (a_1 A + \frac{9}{4} a_3 A^3) \cos \omega_2 t \\
&+ \underbrace{\frac{3}{4} a_3 A^3 \cos(2\omega_1 - \omega_2)t + \frac{3}{4} a_3 A^3 \cos(2\omega_2 - \omega_1)t}_{\text{correct terms for } P_{IM,3}} \\
&+ \frac{3}{4} a_3 A^3 \cos(2\omega_1 + \omega_2)t + \frac{3}{4} a_3 A^3 \cos(2\omega_2 + \omega_1)t \\
&+ \underbrace{\frac{1}{4} a_3 A^3 \cos(3\omega_1 t) + \frac{1}{4} a_3 A^3 \cos(3\omega_2 t)}_{\text{extra terms included in [11] for } P_{IM,3}}
\end{aligned} \tag{A.2}$$

In (A.2), it is seen that the third-order products locate at $2\omega_1 \pm \omega_2$, $2\omega_2 \pm \omega_1$, $3\omega_1$, and $3\omega_2$, respectively, which are illustrated in Figure A.1. By the definition, $\frac{3}{4} a_3 A^3 \cos(2\omega_1 - \omega_2)t$ and $\frac{3}{4} a_3 A^3 \cos(2\omega_2 - \omega_1)t$ are the third-order

intermodulation products. Thus, the output envelope of $P_{IM,3}$, y_3, equals to the sum of the coefficients of these two terms, which is $\frac{3}{2}a_3A^3$.

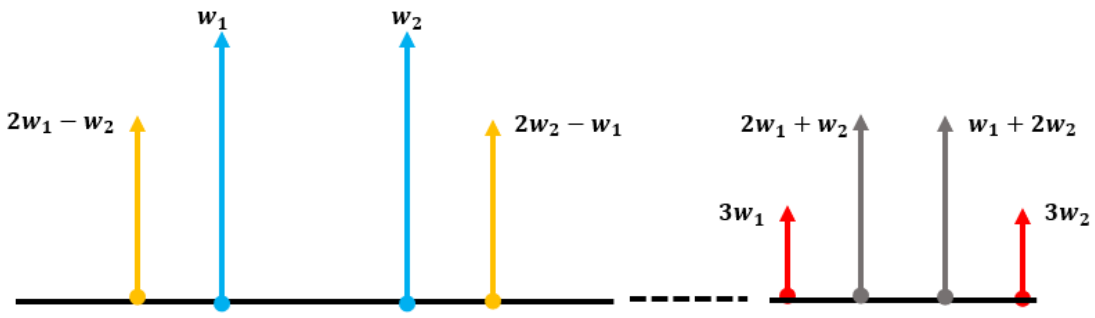

Figure A.1. 3rd-order products with two-tone test.

In [16, eq. (11)], the authors assumed

$$\omega_1 = \omega_c - \Delta\omega \tag{A.3}$$

$$\omega_2 = \omega_c + \Delta\omega \tag{A.4}$$

where ω_c is the carrier frequency of the two-tone signal, and $\Delta\omega = |\omega_c - \omega_1| = |\omega_c - \omega_2|$. However, this approach causes errors. Based on (A.3) and (A.4), the input signal can be rewritten as

$$\begin{aligned} x_{in}(t) &= A\cos(\omega_c - \Delta\omega)t + A\cos(\omega_c + \Delta\omega)t \\ &= 2A\cos(\Delta\omega t)\cos(\omega_c t) \end{aligned} \tag{A.5}$$

Since ω_c is the carrier frequency, the input signal can then be considered as a baseband signal shifted to carrier frequency. Thus, the authors then simplified the input signal by taking the carrier frequency out for amplifications as

$$x_{in}(t) = 2A\cos(\Delta\omega t) \tag{A.6}$$

Inserting (A.6) into (2.12) for n = 2 yields

$$\begin{aligned} x_{out}(t) &= a_1 x_{in}(t) + a_3 x_{in}^3(t) \\ &= a_1 2A\cos(\Delta\omega t) + a_3(2A\cos(\Delta\omega t))^3 \\ &= (2a_1 s + 6a_3 A^3)\cos(\Delta\omega t) + \underbrace{2a_3 A^3 \cos(3\Delta\omega t)}_{P_{IM3}\text{ terms in [11]}} \end{aligned} \tag{A.7}$$

In [16, eq. (11)], the authors considered $2a_3A^3\cos(3\Delta\omega t)$ as the sum of third-order intermodulation products, thus, $2a_3A^3$ as the output envelop of $P_{IM,3}$. By comparing the terms of $P_{IM,3}$ in (A.8) and (A.13), it is known that y_3 in (3.3) equals to $2a_3A^3$ ($=\frac{3}{4}a_3A^3+\frac{3}{4}a_3A^3+\frac{1}{4}a_3A^3+\frac{1}{4}a_3A^3$). It is seen that y_3 not only contains the output envelope of $P_{IM,3}$, but also contains the envelope of the terms which locate at $3\omega_1$ and $3\omega_c$. Similarly, extra terms will be existed in the right of (3.3) while higher-order distortions are considered.